UBE2J2 sensitizes the ERAD ubiquitination cascade to changes in membrane lipid saturation

Authors:

Aikaterini Vrentzou[1], Florian Leidner[2], Claudia C. Schmidt[1,3], Helmut Grubmüller[2], Alexander Stein[1]

Affiliations:

1 Research Group Membrane Protein Biochemistry, Max Planck Institute for Multidisciplinary Sciences, Am Fassberg 11, D-37077 Göttingen, Germany

2 Department of Theoretical and Computational Biophysics, Max Planck Institute for Multidisciplinary Sciences, Am Fassberg 11, D-37077 Göttingen, Germany

3 Current Address: ETH Zürich, Otto-Stern-Weg 3, 8093 Zürich, Switzerland

Correspondence to alexander.stein@mpinat.mpg.de

Abstract

Crosstalk between proteins and lipids forms the basis of homeostatic mechanisms in the endoplasmic reticulum (ER). ER-associated protein degradation (ERAD), a branch of the ubiquitin-proteasome system, regulates ER membrane properties by degrading lipid metabolic enzymes on demand. However, the ERAD components responsible for sensing membrane properties, as well as the underlying the sensing mechanisms, remain largely unknown. Using reconstituted systems with purified ERAD components, we demonstrate that membrane composition modulates the ubiquitination cascade at multiple levels. Early in the cascade, we identify the membrane-anchored E2 UBE2J2 as a sensor for lipid packing. In loosely packed membranes, UBE2J2 is largely inactive as its interaction with the membrane impedes ubiquitin loading. Tighter lipid packing induces a conformational switch in UBE2J2, facilitating interaction with E1. The activity of UBE2J2 governs downstream ubiquitin transfer by the E3 ligases RNF145, MARCHF6, and RNF139, targeting both themselves and the cholesterol biosynthetic enzyme, squalene monooxygenase (SQLE). Additionally, RNF145 directly senses cholesterol levels, rather than lipid packing, resulting in altered oligomerization and activity. Together, these findings indicate that the ERAD machinery integrates multiple lipid signals and suggest that early signal integration by UBE2J2 amplifies lipid-responsive degradation of metabolic enzymes.

Introduction

Biological membranes are complex assemblies of proteins and lipids. Each membranous subcellular compartment exhibits a unique membrane composition necessary to sustain specific biochemical activities (Bigay & Antonny, 2012; Sarmento *et al*, 2023). Different lipid species and their relative abundance influence the dynamics of intermolecular interactions and define collective membrane properties, such as lipid packing and membrane fluidity (Renne & Ernst, 2023). The endoplasmic reticulum (ER) comprises a continuous membrane network characterized by a low content of phospholipids with saturated fatty acyl chains (SFAs) and low cholesterol and sphingolipid concentrations (Reinhard *et al*, 2024; Santinho *et al*, 2024). The resulting loose packing and low rigidity of the ER membrane is optimal for fundamental ER functions such as membrane protein biogenesis (Kamel *et al*, 2022; Nilsson *et al*, 2001; Sharpe *et al*, 2010; van der Does *et al*, 2000), lipid biosynthesis (Haider *et al*, 2018; Manni *et al*, 2018), and trafficking (Karanasios *et al*, 2013; Pathre *et al*, 2003). Intricate regulatory networks maintain the specific properties of the ER membrane. Such adaptive responses require the integration of signals from multiple sensors that monitor various membrane characteristics. Sensor output eventually controls lipid metabolism via changes in gene expression, for example through the membrane property sensors Ire1 (Cho *et al*, 2019; Volmer *et al*, 2013), and Mga2 (Ballweg *et al*, 2020; Covino *et al*, 2016), and/or adjustments in activity and stability of mediators of lipid metabolism by posttranslational mechanisms.

An important post-translational mechanism regulating protein activity is ER-associated protein degradation (ERAD). ERAD executes key homeostatic functions by targeting ER-resident lipid biosynthetic enzymes for degradation, thus adjusting metabolic activity to cellular demand (for recent reviews see (Christianson & Carvalho, 2022; Christianson *et al*, 2023; Stevenson *et al*, 2016)). Specific lipids and collective membrane properties affect ERAD in two ways. First, they influence recruitment of substrates to membrane-embedded ubiquitin ligases (E3s). For example, the key enzymes in the mevalonate pathway for cholesterol biosynthesis, squalene monooxygenase (SQLE) and 3-hydroxy-3-methylglutaryl-coenzyme A reductase (HMGCR), interact with E3s in a lipid-dependent manner. Specifically, SQLE interacts with and is ubiquitinated by the ERAD complex MARCHF6/UBE2J2 in membranes enriched in SFAs and sterols or deprived of its substrate squalene (Chua *et al*, 2019; Gill *et al*, 2011; Huang & Chen, 2023; Stevenson *et al*, 2014; Yoshioka *et al*, 2020; Zelcer *et al*, 2014). HMGCR recruitment to and ubiquitination by several E3s, including RNF145 and RNF139 (also called TRC8), is enhanced by sterol metabolites and mediated by INSIG adaptor proteins (for review see (Schumacher & DeBose-Boyd, 2021)). Second, the membrane composition also modulates flux through ERAD by changing the enzymatic activity of ERAD components, particularly E3 ligases. This notion is

based on the observation that cellular uptake of certain lipids from culture media results in increased autoubiquitination activity and ensuing lower stability of several E3 ligases. For example, high cholesterol levels result in increased autoubiquitination and concomitant destabilization of the E3 RNF145 (Menzies *et al*, 2018; Volkmar *et al*, 2022) and its homolog RNF139 (Irisawa *et al*, 2009; Lee *et al*, 2010), but have the opposite effect on MARCHF6 (Sharpe *et al*, 2019). Besides cholesterol, administration of saturated fatty acids (SFAs) causes destabilization of RNF145 (Volkmar *et al.*, 2022).

How changes in membrane composition are sensed by the ubiquitination machinery and eventually translated into changes in ubiquitination activity is unknown. Most models suggest that membrane-embedded ERAD E3 ligases directly sense membrane composition. For instance, for RNF139 and RNF145 the presence of a sterol-sensing domain similar to that of HMGCR or SCAP has been proposed (Chen *et al*, 2022; Jiang *et al*, 2018; Lee *et al.*, 2010; Menzies *et al.*, 2018; Yan *et al*, 2021a). However, E3s are not the only membrane-associated components in the ubiquitination cascade. Most ubiquitin-conjugating enzymes (E2s) involved in ERAD also associate with the ER membrane, either directly or indirectly. UBE2J2 (Ubc6 in yeast) and UBE2J1 are anchored in the membrane via C-terminal transmembrane segments (TMS) (Cremer *et al*, 2021; Elangovan *et al*, 2017; Tan *et al*, 2019; Wang *et al*, 2009), whereas UBE2G2 (Ubc7 in yeast) is membrane associated via the integral membrane protein AUP1 (similar to Cue1 in yeast) (Ju *et al*, 2010; Klemm *et al*, 2011; Spandl *et al*, 2011). Whether E2 activity is sensitive to specific lipids or modulated by global membrane properties has not been investigated. E2 enzymes interact with RING E3 ligases, which mediate the direct transfer of ubiquitin from the E2 enzyme onto the protein substrate (Christianson *et al*, 2011; Fenech *et al*, 2020). While E3 ligases determine substrate specificity, E2s determine chemoselectivity and linkage specificity of the ubiquitin attachment reaction. For example, UBE2G2 mediates formation of Lys48-linked ubiquitin chains and modifies substrate lysines, whereas UBE2J2 and UBE2J1 also modify serine and threonine residues thus expanding the substrate repertoire. They usually serve as priming E2s that mediate attachment of the first ubiquitin onto the substrate (Chua *et al.*, 2019; Cremer *et al.*, 2021; Swarnkar *et al*, 2024; Wang *et al.*, 2009; Weber *et al*, 2016).

In cellular systems, transcriptional and post-translational homeostatic responses are often difficult to disentangle experimentally, as they are both regulated by lipids (Cook *et al*, 2017; Menzies *et al.*, 2018; Volkmar *et al.*, 2022). In addition, in sequential reactions such as the ubiquitination cascade, membrane properties can affect any membrane-associated enzyme. To overcome these challenges, we used a reconstitution approach with purified human ERAD components in membranes of defined composition, aiming to gain mechanistic insight into how specific lipids and global membrane properties affect ubiquitination during ERAD. We have dissected the ubiquitination cascade into individual reactions and tested the

activity of specific enzymes for lipid sensitivity. We show that lipid packing influences the activity of the E2 UBE2J2 while cholesterol affects the E3 ligase activity of RNF145. Regulation of E2 activity has extensive consequences on downstream reactions mediated by multiple E3 ligases, ranging from E3 autoubiquitination to substrate modification. This study uncovers a previously unknown mechanism by which lipids regulate a ubiquitin conjugating enzyme and suggests that a multi-layered regulation of the ubiquitin cascade is involved in maintaining membrane homeostasis.

Results

UBE2J2 is inactive in ER-like membranes

In order to dissect the effect of different membrane compositions on the ERAD ubiquitination cascade, we first investigated loading of UBE2J2 and UBE2J1 with ubiquitin by the ubiquitin-activating enzyme (E1). To this end, we reconstituted purified and fluorescently labeled full-length E2s into phospholipid vesicles (liposomes) with a low fraction of saturated acyl chains on phospholipids and low cholesterol concentrations that mimicked the ER-membrane(Reinhard *et al.*, 2024; Santinho *et al.*, 2024) (**Extended Data Figure 1A-C).** To follow ubiquitin-loading, we incubated these liposomes with ubiquitin (Ub), E1 and ATP, and analyzed samples by non-reducing SDS-PAGE, which maintains the E2-Ub thioester linkage (**Figure 1A**). Ubiquitin loading of UBE2J2 in ER-like membranes was slow and occurred only over an extended period of incubation (**Figure 1B, C** and **Extended Data Figure 1D, E**). In contrast, in detergent solution UBE2J2 was almost completely loaded within one minute (**Figure 1B, C**), and was additionally auto-ubiquitinated on cysteine residues other than the catalytic C94 (**Extended Data Figure 1F, G**). Suppression of UBE2J2 loading by membrane reconstitution was not due to incorrect UBE2J2 orientation, as the majority of UBE2J2 was correctly oriented in ER-like membranes (**Extended Data Figure 1H, I**), and thus principally accessible to the ubiquitination machinery. Also, low UBE2J2 activity was not due to reduced E1 activity in the presence of liposomes, as high lipid concentrations in the reaction did not affect thioester bond formation between ubiquitin and E1 (**Extended Data Figure 1J**). Furthermore, E1 concentration was not limiting at the concentrations used in our experiments (**Extended Data Figure 1K**). UBE2J2 inactivation in the membrane was reversible, as re-solubilization of proteoliposomes restored UBE2J2 loading (**Extended Data Figure 1L, M**).

Next, we tested ubiquitin loading of the other membrane-anchored E2, UBE2J1. Unlike UBE2J2, UBE2J1 was efficiently loaded with ubiquitin in both detergent solution and ER-like membranes, with the correctly oriented fraction fully loaded within 30 seconds (**Figure 1D, E; Extended Data Figure 1N**). These data indicate that membrane-dependent inhibition of E2 activity is specific to UBE2J2.

Membrane properties tune UBE2J2 activity

As UBE2J2 was largely inactive in an ER-like membrane, we hypothesized that changes in membrane composition could activate it and thus increase ERAD activity. The ER membrane is defined by a high content of unsaturated acyl chains and resulting membrane packing defects. Lipidomic data on ER-derived vesicles from *S. cerevisiae* and mammalian cells, showed that SFAs represent about 25-35% of total acyl chains, with SFAs rarely occupying the sn-2 position and 50-60% of the phospholipids containing unsaturated acyl

chains in both, the sn-1 and sn-2 positions (Reinhard *et al.*, 2024; Santinho *et al.*, 2024). To assess phospholipid saturation effects on UBE2J2, we compared its ubiquitin loading after reconstitution in liposomes with the same phosphatidyl choline (PC): phosphatidyl ethanolamine (PE) molar ratio (80:20), but drastically differing acyl chain composition (**Extended Data Figure 2A, B**). Similar to ER-like membranes that contained 33% SFAs, UBE2J2 activity was low in membranes with 10% SFAs (**Figure 2A, B**). In stark contrast, membranes made solely of palmitoyl-oleyl phospholipids (POPL, 50% SFAs) showed a marked increase in the fraction of UBE2J2 immediately loaded by E1 (**Figure 2A, B**), even at low E1 concentration (**Extended Data Figure 2C**). Raising SFA content to 60% by replacing some POPC with di-palmitoyl PC (DPPC) did not further enhance activity. This activation of UBE2J2 was not due to the decrease in acyl chain length accompanied by replacing oleate (18:1) with palmitate (16:0), but rather due to acyl chain saturation (**Extended Data Figure 2D, E**).

To resolve the rapid kinetics of UBE2J2 loading in membranes with high SFA content, we used a quenched-flow apparatus. In membranes with 60% SFAs, a large fraction UBE2J2 was ubiquitin-loaded within milliseconds, while a second pool was only getting loaded on the minute timescale. By contrast, the fast-loading pool was almost absent in membranes with 10% SFA content (**Extended Data Figure 2F**). These results fit a simple kinetic model, in which UBE2J2 exists in two states, an active and an inactive one; membrane composition affects the interconversion between these states, while the reactivity of the active conformation towards E1 is unaffected by the membrane. Discharge of the loaded state was not accounted for in this model, as it occurs on a minute timescale and is unaffected by membrane composition (**Extended Data Figure 2G, H**).

To further define the sensitivity of UBE2J2 to membrane composition, we incrementally replaced POPL with di-oleyl phospholipids (DOPL). Compared to pure POPL membranes, UBE2J2 activity decreased in membranes with 40% SFAs (20% DOPL) and was further reduced at 35% SFAs (30% DOPL) (**Figure 2C, D**). These findings indicate that UBE2J2 is sensitive to small deviations from the reported physiological content of unsaturated lipids. In contrast, increasing lipid saturation only slightly decreased the fraction of UBE2J1 immediately available for loading (**Extended Data Figure 2I, J**); however, as UBE2J1 orientation also varied in these liposomes (**Extended Data Figure 2K**), this effect may be underestimated. While we did not investigate UBE2J1 loading further, this result suggests that the effect of lipid saturation is specific to UBE2J2.

UBE2J2 may sense changes in membrane composition either through direct interactions with saturated acyl chains or indirectly via saturation-induced changes in global membrane properties. To assess the effect of saturated acyl chains on lipid packing of liposomes, we used the fluorescent probe C-Laurdan, a sensor for lipid packing at the

membrane plane close to the lipid headgroup (Jay & Hamilton, 2017). Dehydration of the membrane due to tighter lipid packing results in a blue-shifted emission of C-Laurdan, expressed as higher generalized polarization. In PC/PE membranes, gradually increasing the content of SFAs resulted in higher C-Laurdan polarization, i.e. tighter lipid packing (**Figure 2E, left**). Thus, UBE2J2 activation correlated with increased lipid packing. To investigate whether UBE2J2 is a membrane property sensor, we induced changes in lipid packing by manipulating the PE and cholesterol content. Compared to PC/PE liposomes, PC-only membranes showed reduced generalized polarization, confirming that PE increases packing (Ballweg *et al.*, 2020; Dawaliby *et al*, 2016) (**Figure 2E, right**). Accordingly, UBE2J2 inactivation in unsaturated membranes was even stronger in the absence of PE (**Figure 2F, G**). However, PE was not required for activation of UBE2J2 in membranes with high SFA content, arguing against a specific effect of its headgroup.

Adding 10 mol% cholesterol to PC/PE liposomes increased generalized polarization of C-Laurdan (**Extended Data Figure 2L**) and slightly enhanced UBE2J2 activity in membranes with 35% SFAs (**Figure 2H, I**), but, had no effect at 60% SFAs. The effect of cholesterol on C-Laurdan polarization was disproportionate to its impact on UBE2J2 activity. We attribute this lack of correlation partly to the limitation of C-Laurdan to accurately probe membrane hydration in the presence of cholesterol (Orlikowska-Rzeznik *et al*, 2023).

Dynamic light scattering showed that variations in membrane composition did not affect (proteo-) liposome size, indicating that differences in membrane curvature do not account for changes in E2 activity (**Extended Data Figure 2M, N)**. Furthermore, protein presence had no significant impact on C-Laurdan polarization (**Extended Data Figure 2O**). Together, these findings reveal that UBE2J2 is sensitive to changes in its membrane environment and suggest that it is a sensor for lipid packing.

Lipid packing affects UBE2J2 conformation

Next, we sought to characterize the molecular mechanism of UBE2J2 inactivation in membranes with packing defects. We hypothesized that membrane properties affect UBE2J2 conformation. We performed limited proteolysis assays on proteoliposomes with either 10% or 60% SFAs using trypsin, and detected N-terminally truncated UBE2J2 fragments that fluoresce at their C-terminus (**Figure 3A**). In both membrane types, trypsin generated a ~10 kDa fragment corresponding to the C-terminal transmembrane segment (TMS) and the disordered linker, confirming that most of UBE2J2 sits in the membrane with the correct orientation. However, at low trypsin concentrations, we observed differential exposure of tryptic sites. In loosely packed membranes (10% SFAs), the N-terminus was more susceptible to proteolysis, producing a ~25 kDa fragment, while it was less accessible in tightly packed membranes (60% SFAs, **Figure 3A, B**). N-terminal tryptic site exposure correlated with low

enzymatic activity. Similarly, in ER-like vesicles with 10 mol% cholesterol, in which UBE2J2 was inactive, the N-terminus was readily cleaved, whereas cleavage was subdued in POPL liposomes in which UBE2J2 was active (**Extended Data Figure 3A)**.

As a second indicator of conformational differences in different membrane environments, we assessed the propensity of UBE2J2 to dimerize or oligomerize. To this end, we measured fluorescence resonance energy transfer (FRET) between UBE2J2 molecules labelled at the C-terminus either with the donor fluorophore Alexa Fluor 488 ($UBE2J2_{A488}$) or with the acceptor fluorophore Alexa Fluor 594 ($UBE2J2_{A594}$). We found significantly higher FRET signal in membranes with 60% SFAs compared to those with 10% SFAs (**Figure 3C, D**). Liposomes containing only donor or only acceptor, showed minimal emission at 614 nm upon excitation at 480 nm, and low, lipid-independent FRET ratios (**Figure 3C, D and Extended Data Figure 3B**). Thus, UBE2J2 transmembrane segments are more closely positioned in tightly packed membranes. This increased propensity for dimerization was confirmed by crosslinking assays. When UBE2J2 liposomes were incubated with the bifunctional cysteine crosslinkers 1,4-bis-maleimidobutane (BMB) or bis-maleimidoethane (BMOE), we observed more dimer- and oligomer-formation in 60% SFAs membranes than in 10% SFAs membranes (**Figure 3E**).

Then, we tested the effect of higher local UBE2J2 concentration on its enzymatic activity. Raising UBE2J2 content in liposomes (higher protein to lipid ratio, P/L) alleviated its activity inhibition in unsaturated membranes (**Figure 3F, G**), a response dependent on its cytosolic region, but not its catalytic activity. At these higher concentrations, UBE2J2 crosslinking increased and became less sensitive to SFA content (**Extended Data Figure 3C**), indicating that dimerization correlates with high activity. However, UBE2J2 dimerization does not appear to directly enhance catalytic activity or be required for it, because soluble UBE2J2 lacking the TMS ($sUBE2J2_{1-226}$) exhibited fast ubiquitin loading kinetics but no dimerization (**Extended Data Figure 3D-F**). Instead, dimerization likely alleviates UBE2J2 inactivation indirectly by promoting an active conformation, akin to the effect of tight lipid packing. In line with this notion, reconstitution of UBE2J2 at high P/L ratios reduced N-terminal accessibility even in loosely packed membranes, similar to the pattern seen in saturated membranes (**Extended Data Figure 3G**). As dimeric UBE2J2 is unlikely to be the functional unit, dynamic disassembly of dimers may precede E1 interaction and ubiquitin loading.

UBE2J2 senses lipid packing via its cytosolic region

Next, we investigated the structural elements in UBE2J2 mediating its lipid sensitivity. Membrane anchoring was essential for this responsiveness, as soluble UBE2J2 was loaded rapidly with fluorescently labelled ubiquitin and was unaffected by the presence

of liposomes (**Extended Data Figure 4A**). To pinpoint regions involved in membrane sensing, we analyzed chimeric UBE2J2 variants in which the TMS and/or the disordered linker were replaced with corresponding regions from UBE2J1 (**Extended Data Figure 4B**). Lipid saturation still activated these UBE2J2 variants (**Figure 4A, B**). Similarly, fusing the cytoplasmic part of UBE2J2 to the TMS of synaptobrevin 2 (Syb2, **Extended Data Figure 4B, C**), did not abolish lipid sensitivity. Conversely, UBE2J1 chimeras incorporating the TMS or linker of UBE2J2 did not acquire lipid sensitivity (**Extended Data Figure 4D-F**). Thus, membrane anchoring is required, but neither the TMS nor the disordered linker of UBE2J2 contains specific lipid sensing elements. We conclude that the UBC domain is primarily responsible for sensing lipid packing, though general physicochemical properties shared by the disordered linkers of UBE2J1 and UBE2J2 may also contribute.

We hypothesized that the cytosolic region of UBE2J2 associates with membranes exhibiting packing defects through hydrophobic interactions. To disrupt such interactions, we used the detergent *n*-octyl-β-D-glucoside (OG). At low concentrations, OG does not solubilize membranes (**Extended Data Figure 4G**), but increases lipid packing by intercalating in the outer leaflet of proteoliposomes (Heerklotz, 2008) (**Extended Data Figure 4H**). In unsaturated membranes, low OG concentrations accelerated UBE2J2 ubiquitin loading (**Figure 4C, D**), whereas activity in saturated membranes was largely insensitive to OG (**Extended Data Figure 4I**). This OG-induced activation correlated with a conformational change: Limited proteolysis of loosely packed liposomes (10% SFAs) treated with 2.6 mM OG (~7.5 times below the critical micellar concentration) showed a cleavage pattern similar to that seen in saturated membranes, whereas the cleavage pattern in tightly packed membranes was unaffected (**Figure 4E**). Together, these observations support the existence of hydrophobic interactions between the cytoplasmic region of UBE2J2 and membranes with packing defects.

Molecular dynamics simulations identify a potential membrane interacting region

To identify potential membrane-interacting regions in the UBC domain and better understand the conformational dynamics of UBE2J2 in the membrane, we performed molecular dynamics simulations of the membrane-embedded protein. The simulation system was designed to be large enough to accommodate the dynamics of the disordered linker region. Since no well-defined membrane interaction motif was present, protein-membrane interactions were expected to be unspecific and transient, posing a challenge for adequate sampling of conformational space. To address this, we used a coarse-grained representation of the system, using the Martini 3 force field (Souza *et al*, 2021).

UBE2J2 was simulated in ER-like membranes, or PC/PE membranes with either 10% of 60% SFAs. For each condition, 10 replicates were simulated for at least 20 µs.

Comparison of the different membranes showed that reducing SFA content from 60% to 10% significantly increased the probability of encountering larger lipid packing defects, while ER-like membranes (33% SFAs and 10% cholesterol) displayed an intermediate effect (Gautier *et al*, 2018), indicating that the simulated membranes exhibited the expected physicochemical properties (**Extended Data Figure 5A**). In all conditions, we observed reversible association of the UBC domain with the membrane. To quantify how lipid composition influences UBC domain association, we calculated the number of contacts between the UBC domain (residues 1–168) and the membrane. The contact distribution was qualitatively similar across all conditions, with two main peaks: one at zero contacts (unbound state) and another at approximately 30 contacts (bound state, **Figure 4F**). To distinguish membrane-bound and -unbound populations, we modeled the contact data as a mixture of Poisson distributions. Across all conditions, a four-component model best fit the data, representing unbound, weakly bound (mean ~ 8 contacts), bound (~ 30 contacts), and tightly bound (~55 contacts) states. The population size of each conformation varied significantly with membrane composition.

Based on experimental observations, we expected that increased lipid packing would favor the unbound state. In the simulations, we also found that the ratio of bound to unbound conformations depended on membrane lipid composition (**Extended Data Figure 5B**), albeit to a smaller extent than indicated by biochemical experiments. In ER-like and 10% SFA membranes, the UBC domain adopted the bound conformation 61% of the time, compared to 54% in 60% SFA membranes. To determine which residues mediate membrane binding, we calculated the lipid contact frequency for each UBE2J2 residue (**Figure 4G, H**). Interactions were centered around a few hydrophobic residues on the UBC surface, particularly M1, M53, F100, and F137. Notably, these interactions clustered around the active site and N-terminus, rather than being uniformly distributed, suggesting a certain degree in specificity of the UBC domain–membrane interactions.

F137E mutation desensitizes UBE2J2 to lipid packing

We focused our experimental validation of these candidate regions on aromatic amino acids, as their side chains have often been implicated in lipid sensing processes (Ballweg *et al.*, 2020; Cho *et al.*, 2019; Covino *et al.*, 2016). Strikingly, substitution of F137 with a negatively charged residue (UBE2J2^{F137E}) rendered UBE2J2 insensitive to lipid packing defects (**Figure 4I, J**). In contrast, the F137Y mutant remained susceptible to inactivation by packing defects, similarly to the wild type protein (**Extended Data Figure 5C**). Intriguingly, when UBE2J2^{F137E} was reconstituted in membranes exhibiting packing defects, it showed a tryptic digestion pattern reminiscent of wild type UBE2J2 reconstituted in highly saturated membranes; specifically, the N-terminus was less susceptible to

proteolysis (**Extended Data Figure 5D** and **Figure 3A**). These results suggest that the F137E mutant adopts an active conformation independent of the membrane composition. In contrast, mutation of another aromatic residue within the catalytic center, F100A, did not affect UBE2J2 inactivation in unsaturated membranes (**Extended Data Figure 5C**).

We reasoned that association of the cytosolic region of UBE2J2 with the membrane impairs its interaction with E1, thereby inhibiting ubiquitin loading. To test this, we analyzed UBE2J2–E1 crosslinking using the cysteine crosslinker BMOE, and observed that crosslinking efficiency was much lower in unsaturated membranes compared to saturated ones (**Figure 4K, left**). Notably, the same low OG concentrations that induced conformational changes in UBE2J2 also restored its interaction with E1 (**Figure 4H, right**). Consistently, interaction of the lipid-insensitive UBE2J2^{F137E} mutant with E1 was also enhanced (**Extended Data Figure 5E**), in line with its observed activity and conformation in the membrane. Thus, UBE2J2 conformation defines its capacity to interact with E1 and undergo ubiquitin loading.

Collectively, these findings indicate that UBE2J2 adopts an auto-inhibitory conformation in membranes with packing defects. Hydrophobic interactions between its cytosolic region and the membrane hinder the recruitment of the E1 enzyme. In contrast, tight lipid packing disfavors these interactions, enabling efficient UBE2J2 loading.

UBE2J2 activity instructs downstream reactions in the ubiquitination cascade

In the ER, UBE2J2 partners with several RING domain containing E3 ligases. It promotes degradation of certain RNF139 substrates, including the tail-anchored protein HO-1, the misfolded cytosolic protein CL-1 and HLA class I molecules during viral immune evasion (Stefanovic-Barrett *et al*, 2018; van de Weijer *et al*, 2017b). Loss of UBE2J2 increases steady-state levels of RNF139, indicating a role in RNF139 autoubiquitination (van de Weijer *et al*, 2017a). Similarly, UBE2J2 collaborates with MARCHF6 to control the stability of MARCHF6 itself and its substrates, including the sterol biosynthetic enzyme SQLE (Sharpe *et al.*, 2019; Stefanovic-Barrett *et al.*, 2018; Tan *et al.*, 2019). To characterize E2-E3 collaboration biochemically, we purified and fluorescently labeled the E3 ubiquitin ligases RNF139, RNF145 and MARCHF6 for reconstitution into liposomes and also purified UBE2G2 and an engineered variant of its co-factor AUP1 (TM_{Cue1}-$AUP1_{271-410}$) (**Extended Data Figure 6A-H**).

To analyze E3 activity in cooperation with UBE2J2 and UBE2G2, we measured E3 autoubiquitination. With UBE2J2 alone, all tested E3s were autoubiquitinated, confirming its collaboration with RNF139 and MARCHF6 and revealing a novel functional interaction with RNF145 (**Extended Data Figure 6I-K**). Based on the molecular weight shifts, UBE2J2 primarily mediated multiple mono-ubiquitinations or the formation of short chains, while UBE2G2 generated longer, mainly K48-linked ubiquitin chains (**Extended Data Figure 6L)**,

as reported before (Bocik *et al*, 2011; Liu *et al*, 2014). When both E2s were present, only long chains were observed, indicating that UBE2J2-initiated mono-ubiquitination is efficiently extended by UBE2G2. Thus, UBE2J2 acts as a priming E2, similar to Ubc6 in yeast (Schmidt *et al*, 2020; Swarnkar *et al.*, 2024; Weber *et al.*, 2016). In addition, most ubiquitin attachments on RNF139 were on serine or threonine residues, as indicated by the sensitivity to sodium hydroxide (NaOH) (Ferri-Blazquez *et al*, 2023) (**Extended Data Figure 6M**), corroborating that UBE2J2 mediates non-canonical ubiquitination (Swarnkar *et al.*, 2024).

Next, we tested whether the lipid-responsiveness of UBE2J2 affects downstream reactions in the ubiquitination cascade. We found that autoubiquitination of RNF145 was enhanced in membranes rich in saturated phospholipids (**Figure 5A, B**) as was RNF145-mediated ubiquitination of UBE2J2 on non-cysteine residues (**Figure 5A, C, Extended Data Figure 7A**). Similar lipid-dependent effects were seen for RNF139 autoubiquitination and MARCHF6-mediated UBE2J2 ubiquitination (**Extended Data Figure 7B-E**).

Since all three ubiquitin ligases responded similarly to lipid saturation, these results suggest that UBE2J2 reactivity dictates E3 autoubiquitination. To determine whether membrane saturation also directly affects E3 ligase activity, we measured RNF145 autoubiquitination in the presence of soluble UBE2J2, whose loading is insensitive to membrane composition (**Extended Data Figures 3E and 4A**). Under these conditions, RNF145 autoubiquitination was unaffected by lipid saturation (**Figure 5D**). Furthermore, we assessed the lipid-sensitivity of E3-mediated discharge of ubiquitin from UBE2G2 onto free ubiquitin. Proteoliposomes containing AUP1 and either RNF145, RNF139, or MARCHF6 were incubated with purified, ubiquitin-loaded UBE2G2 (**Extended Data Figure 7F**) and free ubiquitin. The rate of di-ubiquitin formation was comparable across different lipid compositions for all E3s tested (**Extended Data Figure 7G**). Together, these data indicate that membrane saturation affects E3 activity only indirectly, by modulating UBE2J2.

We next investigated whether lipid-responsiveness of UBE2J2, in concert with its E3 partner, impacts substrate ubiquitination. Since SQLE ubiquitination depends on UBE2J2 and MARCHF6, and is enhanced by lipid saturation in mammalian cells (Huang & Chen, 2023; Stevenson *et al.*, 2014), we purified and reconstituted fluorescently labeled human SQLE into liposomes with varying SFA content (**Extended Data Figure 8A, B**). MARCHF6- and UBE2J2-mediated SQLE ubiquitination was more efficient in membranes with 60% SFAs than in those with 10% SFAs, (**Figure 5E, F**). This effect specifically required full length, membrane-anchored UBE2J2 (**Figure 5G**), demonstrating that UBE2J2 governs the observed differences in SQLE ubiquitination. Under these experimental conditions, we did not detect any effect of saturation-induced conformational changes in SQLE on its ubiquitination

independent of UBE2J2, contrary to previous hypotheses(Chua *et al*, 2017; Stevenson *et al.*, 2014).

As UBE2J2 adopts different conformations depending on the membrane environment, we hypothesized that these dynamics not only affect interaction with E1, but also with E3 ligases. To assess this, we performed co-immunoprecipitation assays with proteoliposomes containing ALFA-tagged RNF145, UBE2J2, and Syb2 as a non-interacting control. After solubilization and precipitation of RNF145-ALFA, we found that significantly more UBE2J2 co-purified with RNF145-ALFA from membranes with 60% SFAs, compared to those with 10% SFAs (**Figure 5H, I**). Syb2 did not co-purify under either condition, confirming the specificity of the assay. Co-purification required co-reconstitution of UBE2J2 and RNF145 within the same membrane, ruling out post-solubilization interactions (**Extended Data Figure 8C**). Moreover, immunoprecipitation of intact liposomes without prior solubilization showed equal co-reconstitution efficiencies, indicating that differences in co-purification reflect membrane-induced changes in protein interactions (**Figure 5H, I**).

The influence of the membrane environment on UBE2J2–E3 interactions depended on protein concentration. An 8-fold increase in membrane protein concentration abolished the lipid sensitivity of UBE2J2–RNF145 binding (**Extended Data Figure 8D**). Similarly, at higher protein levels, the effects of lipid saturation on RNF145 autoubiquitination and MARCHF6-mediated SQLE ubiquitination were diminished (**Extended Data Figure 8E-G**). These results suggest a binding equilibrium between UBE2J2 and its cognate E3 ligase exists in both tightly and loosely packed membranes, and that high local E3 concentrations can overcome the inhibitory effect of packing defects on E2-E3 interactions (**Extended Data Figure 8H**). E3–bound UBE2J2 remains active even in less densely packed membranes, while packing defects otherwise stabilize an inactive UBE2J2 conformation. Thus, lipid saturation impacts not only UBE2J2 loading but also downstream reactions in the ubiquitination cascade.

Cholesterol affects auto-regulation of the E3 ligase RNF145

Finally, we wanted to determine whether the aggregate activity of an E2/E3 pair can integrate multiple lipid signals – specifically, lipid saturation and cholesterol levels. Supplementing culture media with excess cholesterol reduces RNF145 and RNF139 steady-state levels through both transcriptional repression and increased proteasomal degradation (Menzies *et al.*, 2018) (Irisawa *et al.*, 2009; Lee *et al.*, 2010 and **Extended Data Figure 9A, B**). For RNF145, this degradation requires its own E3 ligase activity (Menzies *et al.*, 2018). To distinguish direct effects of cholesterol on RNF145 activity from indirect effects mediated through UBE2J2, we used soluble UBE2J2. Under these conditions, cholesterol enhanced RNF145 auto-ubiquitination in membranes with ER-like SFA levels (**Figure 6A, B**). Likewise, cholesterol also increased RNF145 auto-ubiquitination when full-length UBE2J2

was present in membranes with 60% SFAs – a setting in which UBE2J2 ubiquitin loading is unimpeded by packing defects and not responsive to cholesterol (**Figure 6C, D, cf. Figure 2I**). A weaker effect was observed when measuring RNF145 auto-ubiquitination in the presence of AUP1 and UBE2G2 (**Extended Data Figure 9C, D**). Together, these results indicate that cholesterol directly promotes RNF145 activity, while lipid saturation regulates it indirectly, through UBE2J2.

Cholesterol did not directly modulate E3 activity of RNF145, as the discharge of ubiquitin from UBE2G2 by RNF145 was unaffected by the presence of cholesterol (**Extended Data Figure 9E**). However, cholesterol increased RNF145 oligomerization, an effect independent of SFA content (**Figure 6E, F**), which may enhance intermolecular (in-trans) auto-ubiquitination. In reactions containing both UBE2J2 and UBE2G2, cholesterol slightly increased polyubiquitination of a catalytically inactive RNF145 (C537, 540S, $RNF145^{CS}$) mutant by active RNF145 (**Extended Data Figure 9F, G**). In the absence of a catalytically active RNF145, some $RNF145^{CS}$ was modified by a mono-ubiquitin. Collectively, these results suggest that cholesterol may influence RNF145 auto-ubiquitination by promoting RNF145 self-association and in-trans auto-ubiquitination.

Discussion

ERAD plays an important role in maintaining the identity of the ER membrane, defined by a specific proteome and lipidome. On the protein level, ERAD mediates degradation of proteins that are mistargeted in different ER domains and contact sites (Foresti *et al*, 2014; Khmelinskii *et al*, 2014; Ruggiano *et al*, 2016; Zhou *et al*, 2020). At the lipid level, it regulates the abundance of many lipid-metabolizing enzymes, thus influencing membrane composition (Gill *et al.*, 2011; Avci *et al*, 2024; Schumacher & DeBose-Boyd, 2021; Volkmar *et al.*, 2022). However, how changes in membrane composition are sensed and translated into differential degradative outcomes is unclear. In this study, we identified protein components of the ERAD ubiquitination cascade with membrane sensing features and characterized their mechanisms of signal integration using reconstituted system with purified proteins and defined lipid compositions. We show that membrane composition modulates the ubiquitination machinery at several stages.

At the E2 level, we identify UBE2J2 as a sensor for lipid packing (**Figure 7**). In loosely packed membranes, UBE2J2 adopts conformations in which its cytosolic region associates with membranes exhibiting packing defects, preventing E1 recruitment and loading with ubiquitin. This inactivation can be overcome either by UBE2J2 dimerization or association with a cognate E3 ligase in membrane regions enriched in ERAD factors, or by increased phospholipid saturation, which reduces packing defects and promotes an active UBE2J2 conformation. Of note, unlike other property sensors such as Mga2, IRE1, and PERK (Ballweg *et al.*, 2020; Volmer *et al.*, 2013), which sense membrane properties through elements in transmembrane segments, UBE2J2 relies on its cytosolic UBC domain. Furthermore, unlike for Mga2, IRE1 and PERK, dimerization is not strictly required for UBE2J2-E1 interaction, but rather promotes activity by stabilizing a conformation compatible with E1 interaction.

At the E3 level, RNF145 has been proposed to be directly sensitive to cholesterol levels (Menzies *et al.*, 2018). In agreement with this, we find that cholesterol enhances RNF145 auto-ubiquitination, independent of the E2 enzyme and lipid saturation, possibly by inducing RNF145 dimerization. This suggests that cholesterol could also affect the RNF145 interactome more broadly, as shown for its interaction with INSIG and subsequent HMGCR recruitment and ubiquitination (Jiang *et al.*, 2018; Menzies *et al.*, 2018). The mechanism of cholesterol sensing by RNF145 remains unresolved. It may involve direct cholesterol binding to a putative sterol-sensing domain (SSD) situated in its N-terminal transmembrane domain (Jiang *et al.*, 2018; Menzies *et al.*, 2018), although this SSD differs structurally from those in SCAP and HMGCR (**Extended Data Figure 10A, B**). Alternatively, RNF145 might sense cholesterol levels indirectly, via the impact of cholesterol on global membrane properties such as membrane thickness, fluidity and packing. However, our data do not support a direct

sensing of membrane fluidity as previously proposed (Volkmar *et al.*, 2022). Although increased lipid saturation raises RNF145 auto-ubiquitination, in agreement with its destabilization in cells (Volkmar *et al.*, 2022), we propose this is due to enhanced UBE2J2 activity in saturated membranes. Consistent with this, palmitic acid treatment reduces UBE2J2 levels in cells, likely reflecting increased autoubiquitination.

Regulation of ERAD activity via UBE2J2 is an attractive model for several reasons. First, inactivation of UBE2J2 in the ER membrane could prevent non-specific ubiquitination by its highly reactive catalytic domain, while conditional activation could stimulate a generalized ERAD activation. Through cooperation with several E3 ligases (MARCHF6, RNF139, RNF145) UBE2J2 can influence the turnover of many lipid-metabolic enzymes (Avci *et al*, 2024; Jo *et al*, 2011; Menzies *et al.*, 2018; Volkmar *et al.*, 2022; Zelcer *et al.*, 2014), similar to SQLE in our reconstituted system. This regulation can be temporal (i.e. under ER stress) or spatial, with constitutive UBE2J2 activity in ER subdomains with tight lipid packing (Okamoto *et al*, 2012; Shen *et al*, 2017; Weigel *et al*, 2021) or high abundance of ERAD components. Second, UBE2J2 catalyzes attachment of the first ubiquitin, a rate-limiting step for chain formation (Lips *et al*, 2020; Mehrtash & Hochstrasser, 2022; Pierce *et al*, 2009; Weber *et al.*, 2016), so that its regulation by membrane properties determines overall substrate processing kinetics. Third, UBE2J2 uniquely mediates not only lysine ubiquitination, but can also attach ubiquitin to serine and threonine (Chua *et al.*, 2019; Wang *et al.*, 2009). Therefore, activation of UBE2J2 under specific conditions would lead to an expansion of the substrate repertoire of several ligases. Finally, additional direct regulation at the E3 level enables ERAD to integrate multiple signals, allowing for specific adjustment of activity toward distinct substrate sets defined by the E3 involved.

Acknowledgements

We thank Iris Bickmeyer for excellent technical assistance, Reinhard Jahn, Alex Faesen and Tayfun Hazar Eyyuboğlu for comments on the manuscript, and Sonja Lorenz, Ivo Feussner and Blanche Schwappach for discussions. Furthermore, we thank Marina Rodnina for providing access to a quenched-flow apparatus, and Olaf Geintzer for helping with measurements. We also thank the Facility for Light Microscopy at the MPI-NAT and Peter Lenart for technical support. This work was supported by the Deutsche Forschungsgemeinschaft SFB1190, P15 and by the European Research Council under the Horizon2020 research and innovation program (grant # 677770) (both to AS).

Author contributions

A.V. carried out and analyzed all biochemical experiments. F.L. carried out and analyzed molecular dynamic simulations, C.S. established the protocols for March6 purification. A.S. conceived and supervised this work. H.G. supervised the molecular dynamic simulations. A.V. and A.S. wrote the original draft of the manuscript, all authors contributed to revision and editing of the manuscript

Material and Methods

Molecular cloning

Plasmids for protein expression in *Escherichia coli* (*E. coli*) were cloned using commercially available kits for Gibson assembly and site directed mutagenesis (New England Biolabs, NEB). Plasmids for protein expression in *S. cerevisiae* were generated by GoldenGate assembly (NEB) based on (Lee *et al*, 2015). Protein identifiers and expression plasmids are summarized in Tables 4 and 5. Expression plasmids for RNF145, RNF139 and MARCHF6 were toxic for bacterial growth. Final assemblies were therefore directly transformed in yeast.

Protein expression and membrane fractionation of *E. coli*

Protein expression in *E. coli* was performed using BL21-CodonPlus (DE3)-RIPL cells (Agilent). Protein expression in Terrific Broth(Sambrook & Russell, 2001) was induced with 0.5 mM IPTG for 16 hours at 18 °C, shaking at 130 rpm. Bacterial pellets were harvested by centrifugation at 4000xg for 20 min at 4°C, and resuspended by homogenization in lysis buffer containing 50 mM Tris/HCl pH 7.8, 500 mM NaCl, 30 mM imidazole, 200 mM sucrose, 1 mM PMSF. Bacterial cells were mechanically lysed by three passages through a high-pressure microfluidizer at 16 bar. For soluble proteins, the lysate cleared by was ultracentrifugation for 30 min, 40k rpm, using a Ti45 rotor. For membrane proteins, lysate was precleared by centrifugation at 4000xg for 15 min, then a crude membrane pellet was obtained by ultracentrifugation as above. The membrane pellet was washed once in lysis buffer and the ultracentrifugation step was repeated. Membranes were stored in lysis buffer at -80°C.

Protein purification from E. coli

Membrane fractions were solubilized for 1 hour rotating at 4°C in purification buffer (50 mM Tris/HCl pH 7.8, 500 mM NaCl, 30 mM imidazole, 200 mM sucrose) containing 1% (w/v) detergent and 1 mM PMSF. Solubilized proteins were separated by insoluble material by ultracentrifugation as above. Affinity purification was performed using HisPur Ni-NTA agarose resin (Thermo) and elution was performed by incubation of protein-bound beads with 1 µM Ulp1 for 30 minutes at 4°C.

UBE2J2, UBE2J1 and variants: Membrane fractions of UBE2J2 variants were solubilized in 1% (w/v) DDM. After affinity purification, proteins were fluorescently labeled and further purified by size exclusion, using a Superdex 200 Increase 10/300 GL column equilibrated in 20 mM Hepes/NaOH pH 7.4, 400 mM NaCl, 200 mM Sucrose, 0.5 mM TCEP containing 0.03% (w/v) DDM.

Soluble UBE2J2 and UBE2G2: After affinity purification, proteins were further purified by size exclusion, using a HiLoad 16/600 Superdex 75 pg column, equilibrated in 20 mM Hepes/NaOH pH 7.4, 200 mM NaCl, 200 mM Sucrose, 0.5 mM TCEP.

AUP1: Membrane fraction containing TM_{Cue1}-$AUP1_{271-410}$ was solubilized in 1% DM. After affinity purification, AUP1 was further purified by size exclusion, using a Superdex 200 Increase 10/300 GL column equilibrated in 20 mM Hepes/NaOH pH 7.4, 300 mM NaCl, 200 mM Sucrose, 0.5 mM TCEP containing 0.2% (w/v) DM.

Protein expression and membrane fractionation of *S. cerevisiae*

For protein expression in yeast a *ubc7* deletion strain derived from BY4742 (OpenBiosystems) with genotype *MATα ura3Δ0 his3Δ1 leu2Δ0 lys2Δ0 ubc7::kanR* was used (Stein *et al*, 2014). The general expression protocol using galactose induction was used as described(Stein *et al.*, 2014). The E1 enzyme Uba1 was expressed in the InvSc1 strain (Invitrogen). Yeast pellets were harvested at 4000 x g for 20 minutes at 4°C, washed once in water, were snap-frozen in liquid N_2 as beads and stored at -80°C.

Lysis of frozen yeast was performed mechanically by cryo-milling, using the Planetary Ball Mill PM 100 (Retsch). Yeast beads were subjected to 10 grinding cycles of 2.5 minutes, including 1 minute of reverse rotation, at 400 rpm. Yeast powder was homogenized in membrane fractionation buffer (20 mM Hepes/NaOH pH 7.4, 400 mM NaCl, 200 mM Sucrose, 1 mM PMSF and 2 µM pepstatin A). Whole cell lysate underwent an ultracentrifugation round at 104350 x g for 20 minutes at 4°C and the pellet containing unbroken cells and cell membranes was again homogenized in membrane fractionation buffer. Lysis was further assisted by a single passage through microfluidizer at a pressure of 6 bar. The unbroken cells and cellular debris were pelleted by centrifugation at 2500 x g for 10 minutes at 4°C. The supernatant containing cell membranes was subject to ultracentrifugation at 204526 x g for 45 minutes at 4°C. The pellet containing the membrane fraction was washed and stored in fractionation buffer at -80°C.

Protein purification from *S. cerevisiae*

Membrane fractions were solubilized for 1 hour rotating at 4°C in purification buffer (20 mM Hepes/NaOH pH 7.4, 400 mM NaCl, 200 mM Sucrose, 0.5 mM TCEP) containing 1% (w/v) detergent and 1 mM PMSF. Solubilized proteins were separated from insoluble material by ultracentrifugation at 204526 x g for 30 minutes at 4°C. Proteins expressed in *S. cerevisiae* harbored a streptavidin binding protein (SBP) purification tag (Keefe *et al*, 2001), at the N- or C-terminus. Affinity chromatography for all proteins was performed using streptavidin agarose resin (SERVA) and elution was performed with 2 mM biotin.

RNF145, RNF139 and variants: Proteins were expressed with an N-terminal SBP tag followed by a $SUMO_{EuB}$ protease cleavage site (Vera Rodriguez *et al*, 2019) and a C-terminal ALFA tag (Gotzke *et al*, 2019). Membrane fractions containing RNF145-ALFA, $RNF145_{CS}$-ALFA, $RNF145_{\Delta RING}$-ALFA, $RNF145_{\Delta RING}$-sfGFP and RNF139-ALFA were solubilized in 1.3% (w/v) GDN. After elution, the SBP-$SUMO_{EuB}$ tag was cleaved off by incubating with 1 µM $Senp_{EuB}$ protease for at least 1 hour at 4°C. Proteins were further purified by size exclusion using a Superose 6 Increase 10/300 GL column in buffer containing 20 mM Hepes/NaOH pH 7.4, 250 mM NaCl, 200 mM Sucrose, 0.5 mM TCEP, 0.006% (w/v) GDN.

MARCHF6: MARCHF6 was expressed with an N-terminal SBP tag followed by a $SUMO_{EuB}$ protease cleavage site (Vera Rodriguez *et al.*, 2019) or C-terminal SBP preceded by a TEV cleavage site and followed by a sortase-labeling sequence. Membrane fractions were solubilized in buffer containing 1% (w/v) DMNG, which was reduced to 0.012% (w/v) during affinity purification. Eluted protein was further purified by size exclusion using a Superose 6 Increase 10/300 GL column in buffer containing 20 mM Hepes/NaOH pH 7.4, 150 mM NaCl, 0.2 mM TCEP, 0.012% (w/v) DMNG.

SQLE: SQLE was expressed with an N-terminal SBP tag followed by a $SUMO_{EuB}$ protease cleavage site (Vera Rodriguez *et al.*, 2019). Membrane fractions were solubilized in buffer containing 1% (w/v) DM, which was reduced to 0.2% (w/v) during affinity purification. Eluted protein was further purified by size exclusion using a Superdex200 Increase 10/300 GL column in buffer containing 20 mM Hepes/NaOH pH 7.4, 250 mM NaCl, 0.2 mM TCEP, 0.2% (w/v) DM.
Uba1 was purified according to (Stein *et al.*, 2014). $Syb2_{A488}$ was purified and fluorescently labeled as described in (Stein *et al*, 2007).

Fluorescent labeling of purified proteins

Purified proteins were covalently modified with a fluorescent dye via a transpeptidation reaction catalyzed by the bacterial Sortase A which mediates the ligation of G-rich sequences at the carboxyl terminus of LPxTG sequences (Popp *et al*, 2009). For N-

terminal labeling, recombinant proteins harbored a GGG sequence at their N-terminus, which was exposed upon proteolytic cleavage of the affinity purification tag and was linked to fluorophore-conjugated CLPETGG peptide. For C-terminal fluorescent labeling, recombinant proteins contained a C-terminal LPETGG sequence which was linked to fluorophore-conjugated GGC peptide. In the labeling reaction, purified proteins were incubated with the fluorophore- conjugated peptide (1: 2.5 molar ratio), 2 µM sortase A and 5 mM $CaCl_2$ for 2 or 16 hours at 4°C. Free peptide and sortase were removed gelfiltration using Superose 6 Increase 10/300 GL or Superdex200 Increase 10/300 GL columns equilibrated to the same buffers as used before.

Preparation of liposomes

Large unilamellar vesicles were generated by reverse phase evaporation (Hernandez *et al*, 2012). In detail, synthetic lipids were mixed at defined molar ratios to a final concentration of 20 mM in chloroform. A dry lipid film was generated by chloroform evaporation at 100 mbar for 5 minutes and at 20 mbar for 30 minutes. Subsequently, lipids were dissolved in 1 mL diethyl-ether, followed by addition of 300 µl liposome buffer (20 mM Hepes/KOH pH 7.4, 150 mM KCl, 5 mM $MgAc_2$). A lipid emulsion was generated by tip sonication. Diethyl ether was removed by evaporation at 500 mbar for 5 minutes, until a gel-like phase was formed. Then, 700 µl liposome buffer was added to a final volume of 1 mL. Liposomes were formed with sequential, one hour-long cycles of diethyl ether evaporation at 300 mbar, 200 mbar and 100 mbar. Uniform liposome size was achieved by filtered extrusion through a 0.4 µm and 0.1 µm poly-carbonate filters (Mini extruder kit, Avanti Polar Lipids). Detailed lipid compositions are described in Table 6.

Protein reconstitution in liposomes

Proteoliposomes were generated as described (Schmidt *et al.*, 2020). Briefly, 4 mM of liposomes were partially solubilized by addition of DM to a final concentration 8.2 mM in a total volume of 100 or 130 µl reconstitution buffer (20 mM Hepes/KOH pH 7.4, 150 mM KCl, 5 mM $MgAc_2$, 0.2 mM TCEP). Purified proteins were added at defined protein to lipid ratios (P/L), and the mixture was incubated for 1 hour at ambient temperature. Detergent was removed in three 20- minute-long incubation cycles with 350 µg/µL Pierce detergent removal resin (DRR) (Thermo Scientific) at ambient temperature. After each cycle, DRR was removed by centrifugation at 2500 x g for 2 minutes using Pierce micro-spin columns (Thermo Scientific).

Flotation assay

Proteo-liposomes were placed at the bottom layer of a density gradient containing 40% (100 µl), 30% (40 µl), 15% (40 µl) and 0% (40 µl) (w/v) Nycodenz in reconstitution buffer (20 mM Hepes/KOH pH 7.4, 150 mM KCl, 5 mM $MgAc_2$, 0.1 mM TCEP). The density gradient was subjected to ultracentrifugation at 55,000 rpm at 4°C in a TLS55 rotor, during which reconstituted proteins co-migrated with lipids at the top, least dense density fractions. Six fractions (36.5 µL each) were collected from the top of the density gradient and analyzed by SDS-PAGE and fluorescence (Li-Cor) or stain-free (BioRad) scanning.

Antibody accessibility assay

Antibody accessibility assays were performed as described previously (Schmidt *et al.*, 2020) using a Tecan Genios Pro microplate reader. First, the basal fluorescence of Alexa Fluor 488-labelled E2 (f.c. 100 nM) in liposomes or detergent was measured using 495/10 nm and 535/25 nm for excitation and emission, respectively. Subsequently, anti-Alexa Fluor 488 polyclonal antibody (A-11094, Invitrogen) was added at a dilution of 1:15 and changes in fluorescence were measured over time. After 10 minutes, liposomes were solubilized by addition of 1% Triton X-100 (1:20 dilution from a 20% stock) and further reduction in

fluorescence was measured until signal was stabilized. The data of these three individual measurements were merged, background fluorescence after detergent addition was subtracted, and data were normalized to maximal basal fluorescence.

Limited proteolysis and protease protection assay

Protease protection assays were used to analyze protein orientation and conformation. Proteoliposomes were incubated with the TEV protease, Ulp1 or trypsin (Roche) at concentrations, temperature and time courses indicated below each experiment. Proteolysis was stopped by addition of 5 mM PefaBloc (Roche) and incubation at ambient temperature for 10 minutes. Subsequently, 4x LDS sample buffer was added, protein samples were heated at 50°C for 10 minutes and analyzed by SDS-PAGE and fluorescence scanning or western blotting.

Dynamic light scattering

The average diameter of (proteo)-liposomes was determined by dynamic light scattering (DynaPro Titan, Wyatt Technology) using the Dynamics V6 software. In brief, (proteo)-liposomes were diluted to a final concentration of 1 mM lipid into buffer containing 20 mM Hepes/KOH pH 7.4, 150 mM KCl, 5 mM MgAc2. Each measurement took place at 25°C, with 3% laser power, including 10 cycles of 10 seconds each.

C-Laurdan measurements

C-Laurdan measurements were performed as described, with minor modifications (Ballweg *et al.*, 2020). Briefly, 0.5 mM liposomes were incubated with 0.5 µM C-Laurdan (R&D systems) in liposome buffer (20 mM Hepes/KOH pH 7.4, 150 mM KCl, 5 mM MgAc2) for 30 minutes at 37°C. Recording of the fluorescence emission spectrum was carried out in a plate reader (BioTek Synergy Neo 2) at 37°C (excitation=375 nm (10 nm range), emission spectrum =400-600 nm (20 nm range) with a 2 nm wavelength step). Generalized polarization (GP) was calculated based on the equation below, where I_{p1} equals the sum of intensity at wavelength range 402-460 nm and I_{p2} equals the sum of intensity at wavelength range 470-530 nm.

$$\mathrm{GP} = \frac{\mathrm{Ip1} - \mathrm{Ip2}}{Ip1 + Ip2}, \qquad -1 < GP < 1$$

Ubiquitin loading assay

Ubiquitin loading assays were performed in ubiquitination buffer (20 mM Hepes/KOH pH 7.4, 150 mM KCl, 5 mM $MgAc_2$, 0.1 mM TCEP). Proteoliposomes containing 50 nM E2 enzyme were incubated at 37°C for 10 minutes prior to addition of the ubiquitination machinery, containing yeast Uba1 at a concentration of 1 µM for UBE2J2 or 4 µM for UBE2J1, 50 µM yeast ubiquitin, 2.5 mM ATP and 0.2 mg/mL BSA. At different timepoints, samples were transferred into 4x LDS sample buffer with or without 6% (v/v) β-mercaptoethanol and were analyzed by SDS-PAGE and fluorescence scanning.

Ubiquitination assay

Ubiquitination assays were performed in ubiquitination buffer (20 mM Hepes/KOH pH 7.4, 150 mM KCl, 5 mM $MgAc_2$, 0.1 mM TCEP). Proteoliposomes containing 50 nM E3 ligase were mixed with the ubiquitination machinery including 0.1 µM yeast Uba1, 50 µM yeast ubiquitin, 0.2 mg/mL BSA on ice. Reactions were placed at 37°C and ubiquitination started by addition of 2.5 mM ATP. At different timepoints, samples were transferred into 4x LDS sample buffer with or without 6% (v/v) β-mercaptoethanol and analyzed by SDS-PAGE and fluorescence scanning.

Quenched-flow and kinetic models

Rapid quenched kinetic analysis was carried out using an RQF-3 quench flow instrument (KinTek Corporation). Equal volumes of reaction solution A, containing 100 nM

$UBE2J2_{DL680}$ in liposomes, and reaction solution B, containing 2 μM Uba1, 100 μM Ubiquitin and 5 mM ATP, both in ubiquitin loading buffer and equilibrated to 37°C, were rapidly mixed. Reactions were quenched using 0.1 M HCl and collected in 4x LDS sample buffer-containing tubes. Samples were analyzed by SDS-PAGE and fluorescence scanning. For the analysis data from Figure 2A, B were included for $t \geq 30s$ and ≤ 10 min.

For kinetic fitting, we assumed a simple mechanism, in which an active and inactive conformation of UBE2J2 (A and B, respectively) interconvert with rates k_1 and k_2, respectively, and only the active conformation can react with k_3 with ubiquitin-loaded E1 to yield C, ubiquitin-loaded Ube2J2, yielding the following set of equations:

$$\frac{d[\mathrm{C}]}{dt} = k_3[\mathrm{A}]$$

$$\frac{d[\mathrm{A}]}{dt} = -k_3[\mathrm{A}] - k_1[\mathrm{A}] + k_2[\mathrm{B}]$$

$$\frac{d[\mathrm{B}]}{dt} = k_1[\mathrm{A}] - k_2[\mathrm{B}]$$

In this model, the starting concentrations $[A]_0$ and $[B]_0$ are determined by

$$\frac{[\mathrm{B}]_0}{[\mathrm{A}]_0} = \frac{k_1}{k_2}$$

and the total concentration of loadable UBE2J2, [T], defined as $[T] = [A]_0 + [B]_0$. This set of equations was solved using a formalism described by Andraos (Andraos, 1999), resulting in

$$\mathrm{C}(t) = T\left[\frac{k_3k_2}{k_1+k_2}\frac{e^{r_1t}-e^{r_2t}}{r_1-r_2} + \frac{k_3k_1}{k_1+k_2}\frac{\frac{e^{r_1t}-1}{r_1}-\frac{e^{r_2t}-1}{r_2}}{r_1-r_2}\right]$$

with

$$r_{1,2} = \frac{-(k_1+k_2+k_3) \pm \sqrt{(k_1+k_2+k_3)^2 - 4k_2k_3}}{2}$$

Global fitting was then performed using the Origin software (Version 2018b, OriginLab Corporation, Northampton, MA, USA), in which k_3 was shared, concentrations expressed as fractions of the total UBE2J2, and T fixed as 0.75. Discharge of UBE2J2 by hydrolysis of the thioester was neglected in this model.

Discharge assays

For discharge of UBE2J2, $UBE2J2_{DL680}$ was loaded with ubiquitin, as described above. Subsequently, ubiquitin loading reactions were quenched by dilution (1:10) into EDTA-containing buffer (20 mM Hepes/KOH pH 7.4, 150 mM KCl, 2 mM EDTA, 0.1 mM TCEP), and discharge was monitored over time.

For discharge of UBE2G2, UBE2G2 was loaded with fluorescently labeled ubiquitin in a reaction containing 73 μM UBE2G2, 3 μM Uba1, 120 μM fluorescent ubiquitin and 2 mM ATP in ubiquitination buffer (20 mM Hepes/KOH pH 7.4, 150 mM KCl, 5 mM $MgAc_2$, 0.1 mM TCEP). After incubation at 37°C for 100 minutes, reaction was stopped by addition of 10 mM EDTA and ubiquitin-loaded UBE2G2 was purified by size exclusion in buffer containing 10 mM MES pH 6.0, 150 mM NaCl, 0.5 mM TCEP. Proteo-liposomes (f.c. 100 nM of E3 ligase) were mixed with 100 μM ubiquitin in buffer containing 20 mM Hepes/KOH pH 7.4, 150 mM KCl, 5 mM $MgAc_2$, 0.1 mM TCEP and were pre-equilibrated at 37°C for 5 minutes. Subsequently, 100 nM ubiquitin-loaded UBE2G2 was added and discharge was

monitored over time. Samples were transferred in 4x LDS sample buffer and analyzed by SDS-PAGE and fluorescence scanning.

Proteoliposome immunoprecipitation assay

Immunoprecipitations took place in buffer containing 20 mM Hepes/KOH pH 7.4, 150 mM KCl, 5 mM $MgAc_2$, 0.1 mM TCEP. Pierce magnetic streptavidin beads (Thermo) were coated with 2 μM biotinylated anti- ALFA or anti- GFP nanobody and, subsequently, free streptavidin was blocked with 0.1 mM biotin-PEG. Nanobody-coated beads were washed and incubated with blocking solution containing 2 mg/mL BSA for five minutes to prevent non-specific interactions. Proteoliposomes used as input were either intact or pre-solubilized with detergent for 30 minutes at ambient temperature. Proteoliposome input containing 0.2 mg/mL BSA was incubated with nanobody-coated beads (bead to input ratio of 1:2) and incubated for one hour at ambient temperature. Beads were washed three times with pull down buffer containing 0.2 mg/mL BSA (and 0.5% (w/v) DM for solubilized liposomes only). Elution was performed with 1 μM Ulp1* to release nanobody-protein complex from coated beads in DM-containing buffer. Samples were analyzed by SDS-PAGE and fluorescence scanning.

FRET assays

Liposomes were reconstituted with donor or acceptor fluorophore-labeled protein at defined protein to lipid ratios. Proteo-liposomes were incubated for 30 minutes at 37°C in liposome buffer 20 mM Hepes/KOH pH 7.4, 150 mM KCl, 5 mM $MgAc_2$, 0.1 mM TCEP containing 0.2 mg/mL BSA. Samples were excited with a wavelength of 480 nm and fluorescence emission spectra were recorded in a plate reader (BioTek Synergy Neo 2) at 37°C.

Cysteine crosslinking

Proteo-liposomes (f.c. 100 nM protein) were incubated with the crosslinker bis(maleimido)ethane (BMOE) or 1,4-bis(maleimido)butane (BMB) (Thermo Scientific) at 25°C for 30 or 45 minutes in buffer containing 20 mM Hepes/KOH pH 7.4, 150 mM KCl, 5 mM $MgAc_2$. Crosslinkers were quenched by addition of 10 mM DTT for 10 minutes at ambient temperature. Then, protein samples were mixed with 4x LDS sample buffer and analyzed by SDS-PAGE and fluorescence scanning.

Protein analysis by SDS-PAGE

SDS-PAGE was performed based on the classical method described by Laemmli (1970). Proteins mixed with LDS buffer (Schägger, 2006) were heated at 50°C for 5 minutes and loaded onto a 4– 20% Mini-PROTEAN® TGX™ or Criterion™ TGX Precast Gel (Bio-Rad). The marker used was the PageRuler™ Plus Prestained Protein Ladder, 10 to 180 kDa (Thermo Scientific). Electrophoresis was performed in 1x Laemmli buffer (3 g/L Tris, 14.4 g/L glycine, 1 g/L SDS). Proteins were visualized using a Gel Doc™ EZ system for stain-free detections or by staining using Instant Blue Coomassie stain (0.008% (w/v) G250 Coomassie Blue G-250, 9.4% (w/v) orthophosphoric acid (85%), 0.25% (w/v) each cyclodextrin (α-, β-, γ-). Fluorescence scanning was performed in an Odyssey DLx imager (Licor) or in a Typhoon™ FLA 7000 (GE).

Western blot

Proteins were transferred from the gel onto a nitrocellulose membrane using the Trans-Blot® Turbo™ semi- dry transfer system (Bio-Rad) according to the manufacturer's guidelines. Nitrocellulose membranes were incubated in blocking solution (5% (w/v) skim-milk powder in Tris-buffered saline containing 20 mM Tris-HCl pH 7.4, 150 mM NaCl, 0.1% (v/v) Tween20 (TBS-T) for 1 hour at ambient temperature. Subsequently, they were incubated with the primary antibody solution (αSBP 1:1000 (MAB10764); αRNF145 1:1000

(HPA036562); αGAPDH (MA515738) 1:2000 in 5% (w/v) skim-milk powder in TBS-T) for 1 hour at ambient temperature or overnight at 4°C. After three 5-minute washes in TBS-T, membranes were incubated with the IRDye conjugated secondary antibody (1:15,000, Li-Cor) for 1 hour shaking at ambient temperature. Washing steps were repeated and fluorescence was detected using an Odyssey scanner (Li-Cor).

Image analysis and quantifications

Quantification of immunoprecipitation assays and western blots was carried out in ImageStudio™ (Li-Cor). Quantification of ubiquitin loading and ubiquitination was performed in FIJI (Schindelin *et al*, 2012). The fraction of modified protein was calculated by normalization of modified band (or lane area) intensity to total lane intensity. Graphs were prepared using the Origin software (Version 2018b, OriginLab Corporation, Northampton, MA, USA).

Mammalian cell culture

HeLa cells were kindly provided by Dr. Sonja Lorenz, MPI-NAT. HeLa cells were cultured in Dulbecco's modified Eagle's high glucose medium (DMEM) supplemented with 10% fetal bovine serum (FBS) and 50 units/ml penicillin-streptomycin. Cultures were maintained in 10 cm plastic culture dishes at 37°C and 5% CO_2.

Manipulation of cholesterol content was performed according to available protocols (Menzies *et al.*, 2018). Briefly, HeLa cells were cultured in complete medium (DMEM containing 5% (v/v) FBS, penicillin, streptomycin) until they reached 70% confluency (~30 hours). Subsequently, complete medium was removed and cells were washed three times with pre-warmed PBS. For sterol depletion, HeLa cells were then cultured in sterol depletion medium (DMEM containing 5% (v/v) LPDS, 50 μM mevalonate, 10 μM mevastatin) for approximately 20 hours. Subsequently, cholesterol was replenished by supplementing the medium with 50 μM cholesterol complexed with β-methyl-cyclodextrin (chol: β-MCD). For preparation of mevalonate, mevalonolactone was hydrolyzed under alkaline conditions by incubation with 2.04 M KOH. The chol:βMCD stock was prepared based on published protocols (Christian *et al*, 1997). First, powdered cholesterol was dissolved in chloroform: methanol solution (1:1) at a final concentration 50 mg/mL. The solvent was removed by rotary evaporation at 100 mbar pressure for 5 minutes and 20 mbar for 30 minutes. The dry lipid film was dissolved by tip sonication in 25 mM βMCD in water to a final cholesterol concentration of 2.5 mM. The solution was incubated overnight at 37°C under rotation, filtered and stored at -20°C.

HeLa cell lysis and total protein extraction

Cells growing on dishes were washed twice with ice cold PBS and were scraped off into PBS on ice. Cell pellets were obtained by centrifugation at 2500xg for 3 min using a benchtop centrifuge at 4°C and resuspended in lysis buffer (50 mM Tris/HCl pH 7.5, 150 mM NACl, 1 mM EDTA, 0.1% (w/v) SDS, 1% (v/v) Triton-X100) supplemented with 1 mM PMSF and protease inhibitor cocktail. After incubation on ice for 40 minutes, unbroken cells and debris were removed by centrifugation at 17,000 x g for 15 minutes. Samples were analyzed by SDS-PAGE and western blotting.

Molecular Dynamics Simulations

Coarse-grained model of full length UBE2J2 embedded in model membranes

Initial coordinates of UBE2J2 were taken from the x-ray structure (PDBID: 2F4W) (Sheng *et al*, 2012). The linker and transmembrane helix were modeled based on the Alphafold2 prediction (Jumper *et al*, 2021). The structure was centered on the transmembrane helix and rotated so that the helix was aligned with the z-axis. Subsequently we used

Martinize2, distributed with version 0.13.0 of the vermouth library to generate the coarse-grained structure and protein topology (Kroon *et al*, 2025). The Martini3-IDP force field was used to assign force field parameters (Souza *et al.*, 2021; Wang *et al*, 2025). Elastic net restrains were applied to the E2 domain (residues 13-170) and transmembrane helix (residues 229-259) (Periole *et al*, 2009). Pairwise distance restraints were applied based on an upper distance cutoff of and 0.9 nm, a lower cutoff distance of 0.5 nm and a force constant of 700 kJ/mol/nm^2. These parameters best reproduced the root mean squared fluctuation of E2 domain in reference all-atom simulations. After generating the initial distance restraints, we removed the restraints on the flexible active site loops (residue 99-103 and 126-129). The protein was subsequently embedded in the model membrane systems using a modified version of the insane2 script. The updated Martini3 lipid parameters and Martini3 cholesterol parameters were used to parameterize the membrane (Borges-Araujo *et al*, 2023; Pedersen *et al*, 2024). Solvent molecules and potassium chloride beads were added. The ion concentration was 150 mM, additional ions were added to neutralize the charge of the system. The Martini3 parameters were used for the water and ion beads, for potassium we used the SQ4 bead recommended in the original Martini3 publication (Souza *et al.*, 2021).

The simulation systems were then subjected to a two-stage energy minimization. First, position restraints were applied to the protein (500 kJ/mol/nm^2) and the phosphate beads of the lipids (100 kJ/mol/nm^2). In the second stage, the system underwent energy minimization without position restraints. Both energy minimizations used the steepest descent algorithm and were carried out to machine precision. After energy minimization, the systems underwent a series of short simulations. The Verlet scheme was used in all simulations. Pairwise interactions were evaluated explicitly up to 1.2 nm. The potential shift method was used for van der Waals (vdW) interactions to shift them to zero at the cutoff, and the reaction field method was used for long-range electrostatic interactions with a dielectric constant of 15. In the first simulation, the systems were simulated for 200 ps, maintaining a constant system volume. An integration timestep of 2 fs was used. The system was coupled to a Berendsen thermostat with a coupling constant of 1 ps and a target temperature of 298 K (DOI: 10.1063/1.448118). Initial velocities were assigned from a Maxwell distribution. In subsequent equilibration simulations, initial velocities were assigned from the final frame of the previous simulations. Position restraints were applied to the backbone and lipid phosphate beads with force constants of 1000 and 200 kJ/mol/nm^2, respectively. The system was simulated for 400 ps in the second simulation. The position restraints were from the previous simulation. The system was coupled to a Berendsen barostat with a target pressure of 1 bar and a coupling constant of 3 ps. Pressure coupling was implemented independently in the xy plane and z direction (semi-isotropic). This simulation was followed by a second NPT simulation in which the force constants of the position restraints were reduced to 500 and 100 kJ/mol/nm^2. The integration time step was increased to 10 fs, and the system was simulated for 25 ns. For the final equilibration simulation, we removed the position restraints fully and increased the integration timestep to 20 fs. We then simulated the system for 100 ns. Additionally, we switched from the Berendsen thermostat and barostat to the C-Rescale barostat and V-Rescale thermostat.(Bernetti & Bussi, 2020) (Bussi *et al*, 2007).

Simulations

The same parameters were used in the production runs as in the final equilibration simulation. Ten replicates were simulated, with initial velocities assigned randomly from a Maxwell distribution. Each replicate was simulated for at least 20 μs.

Analysis

Most analysis utilized tool implemented in GROMACS version 25.1 and custom python scripts build upon MDAnalysis version 2.70 (Naughton *et al*, 2022). Additionally, we used PackMem to calculate membrane defects (Gautier *et al.*, 2018). Packing defects were evaluated on a regular grid with 1 grid spacing. Following the recommended protocol, we used the vdW radius of the coarse-grained beads to determine grid occupancy. Since this value is not provided directly in the Martini3 force field, it was calculated from the self-interactions. Statistical analysis of the packing defect was performed using python.

Table 1 List of lipids for liposome preparation and detergents

Lipids	Full name	Source
DOPC	1,2-dioleoyl-sn-glycero-3-phosphocholine	850375P (Avanti)
POPC	1-palmitoyl-2-oleoyl-glycero-3-phosphocholine	850457P (Avanti)
16:1 (Δ9-Cis) PC	1,2-dipalmitoleoyl-sn-glycero-3-phosphocholine	850358 (Avanti)
DPPC	1,2-dipalmitoyl-sn-glycero-3-phosphocholine	850355P (Avanti)
DOPE	1,2-dioleoyl-sn-glycero-3-phosphoethanolamine	850725P (Avanti)
16:1 PE	1,2-dipalmitoleoyl-sn-glycero-3-phosphoethanolamine	850706 (Avanti)
POPE	1-palmitoyl-2-oleoyl-sn-glycero-3-phosphoethanolamine	850757P (Avanti)
DOPS	1,2-dioleoyl-sn-glycero-3-phospho-L-serine	840035P (Avanti)
Cholesterol	Cholesterol (ovine wool, >98%)	700000P (Avanti)
DM	n-Decyl β-maltoside	Glycon Biochemicals
DDM	n-Dodecyl α-maltoside	Roth
GDN	glyco-diosgenin	Anatrace
DMNG	Decyl Maltose Neopentyl Glycol	Anatrace
OG	n-Octyl β-D-glucopyranoside	Glycon Biochemicals
Triton-X100	Anapoe-X-100	Anatrace

Table 2 List of media and supplements for yeast and bacterial cultures

Medium and supplements	Catalogue number	Company
Yeast Nitrogen Base	C19032801	US Biological Life Sciences
Yeast extract	8013-01-2	Roth
Tryptone/ Peptone	91079-40-2	Roth
CSM (-HTLU)	DCS1389	Formedium
CSM (-U)	DCS0161	Formedium
Histidine	DOC0142	Formedium
Leucine	DOC0154	Formedium
Uracil	DOC0214	Formedium
Tryptophan	DOC0186	Formedium
D (+) -Galactose	A1131	PanReac AppliChem
D (+) -Glucose anhydrous	GLU04	Formedium

Table 3. List of cell culture media and reagents

Reagent	Catalogue Number	Source
DMEM	D6429	Sigma-Aldrich
Lipoprotein-deficient serum (LPDS)	FB-1001L	Biosera
Trypsin/ EDTA	BE17-161E	Lonza
Penicillin/streptomycin	09-757F	Lonza
FBS	P30-8500	PAN biotech

Mevastatin	M2537	Sigma-Aldrich
Mevalonolactone	M4467	Sigma-Aldrich
β-Methyl-cyclodextrin	C4555	Sigma-Aldrich

Table 4 Genes and Uniprot IDs.

Protein	Organism	Protein ID
UBE2J2	*Homo sapiens*	Q8N2K1
UBE2J1	*Homo sapiens*	Q9Y385
RNF145	*Homo sapiens*	Q96MT1
RNF139	*Homo sapiens*	Q8WU17
MARCHF6	*Homo sapiens*	O60337
SQLE	*Homo sapiens*	Q14534
UBE2G2	*Homo sapiens*	P60604
AUP1	*Homo sapiens*	Q9Y679
Uba1	*Saccharomyces cerevisiae*	P22515
Cue1	*Saccharomyces cerevisiae*	P38428
Synaptobrevin 2	*Rattus norvegicus*	P63045

Table 5. List of expression constructs

Construct	Source
pET39 His14-SUMO-UBE2J2-LPETGG	This study
pET39 His14-SUMO-UBE2J2^{C94A}-LPETGG	This study
pET39 His14-SUMO-UBE2J2^{C94only}-LPETGG	This study
K27 His14-SUMO-UBE2J2$_{1-226}$-LPETGG	This study
K27 His14-SUMO-UBE2J2-TM$_{Syb2}$-LPETGG	This study
K27 His14-SUMO-UBE2J2$_{1-180}$-UBE2J1$_{193-318}$-LPETGG	This study
K27 His14-SUMO-UBE2J2$_{1-180}$-UBE2J1$_{193-287}$-UBE2J2$_{228-259}$-LPETGG	This study
pET39 His14-SUMO-UBE2J1-LPETGG	This study
pET39 His14-SUMO-UBE2J1$_{1-192}$-UBE2J2$_{181-227}$- UBE2J1$_{288-}$318-LPETGG	This study
pET39 His14-SUMO-UBE2J1$_{1-192}$-UBE2J2$_{228-259}$ -LPETGG	This study
K27 His14-SUMO-UBE2G2	This study
pET39 His14-SUMO-TM$_{Cue1}$-AUP1$_{271-410}$	This study
pYTK pGal1-SBP-SUMO$_{EuB}$- GGC-RNF145-ALFA	This study
pYTK pGal1-SBP-SUMO$_{EuB}$- GGC-RNF145$_{C537,540S}$-ALFA	This study
pYTK pGal1-SBP-SUMO$_{EuB}$- GGC-RNF145$_{\Delta RING}$-sfGFP	This study
pYTK pGal1-Avi-SUMO*- linker-RNF145-TEV-SBP	This study
pYTK pGal1-SBP-SUMO$_{EuB}$- GGC-RNF139-ALFA	This study
pYTK MARCHF6-TEV-SBP-LPETGG	This study
pYTK SBP-SUMO$_{EuB}$- MARCHF6	This study
pYTK SBP-SUMO$_{EuB}$- SQLE	This study
K27 untagged yeast ubiquitin	This study
pRS426 pGAL1-His14-TEV-Uba1	(Stein *et al.*,

	2014)
pSF1878 His14-TEV-Ulp1* protease	(Frey & Görlich, 2014)
pTG-A326 His14-TEV-Ulp1$_{406-621}$ protease	(Stein *et al.*, 2014)
pAV286 His14-TEV-SENP$_{EuB}$ protease	(Vera Rodriguez *et al.*, 2019)
pRK793 MBP-TEVsite-His7- TEV protease	(Kapust *et al*, 2001)
K27 His-SUMO-Syb2 with C-terminal cysteine (1-117C)	(Schmidt *et al.*, 2020)
His14-AVI-SUMO*-αGFP nanobody	(Pleiner *et al*, 2015)
His14-AVI-SUMO*- αALFA nanobody	This study

Table 6. Compositions of liposomes used in this study.

Lipid species (mol%)		Lipid mix (SFA content)									
	33% SFA (ER-like)	10% SFA	35% SFA	40% SFA	50% SFA	60% SFA	35% SFA +cholesterol	60% SFA +cholesterol	10% SFA (PC only)	60% SFA (PC only)	10% SFA (16 carbons)
DOPC		60	10				6.7		80		
16:1 PC											60
POPC	60	20	70	80	80	60	66.7	56.7	20	80	20
DPPC						20	16.7	16.7		20	
DOPE	20	20	20	20							
16:1 PE											20
POPE					20	20		16.7			
DOPS	10										
Cholesterol	10						10	10			

References

Andraos (1999) A Streamlined Approach to Solving Simple and Complex Kinetic Systems Analytically. *Journal of Chemical Education* 76: 1578

Avci D, Heidasch R, Costa M, Lüchtenborg C, Kale D, Brügger B, Lemberg MK (2024) Intramembrane protease SPP defines a cholesterol-regulated abundance control of the mevalonate pathway enzyme squalene synthase. *J Biol Chem* 300(2): 105644

Ballweg S, Sezgin E, Doktorova M, Covino R, Reinhard J, Wunnicke D, Hänelt I, Levental I, Hummer G, Ernst R (2020) Regulation of lipid saturation without sensing membrane fluidity. *Nature Communications* 11: 756

Bernetti M, Bussi G (2020) Pressure control using stochastic cell rescaling. *J Chem Phys* 153: 114107

Bigay J, Antonny B (2012) Curvature, lipid packing, and electrostatics of membrane organelles: defining cellular territories in determining specificity. Dev Cell 23:886-95

Bocik WE, Sircar A, Gray JJ, Tolman JR (2011) Mechanism of polyubiquitin chain recognition by the human ubiquitin conjugating enzyme Ube2g2. *J Biol Chem* 286: 3981-3991

Borges-Araujo L, Borges-Araujo AC, Ozturk TN, Ramirez-Echemendia DP, Fabian B, Carpenter TS, Thallmair S, Barnoud J, Ingolfsson HI, Hummer G *et al* (2023) Martini 3 Coarse-Grained Force Field for Cholesterol. *J Chem Theory Comput* 19: 7387-7404

Bussi G, Donadio D, Parrinello M (2007) Canonical sampling through velocity rescaling. *J Chem Phys* 126: 014101

Chen H, Qi X, Faulkner RA, Schumacher MM, Donnelly LM, DeBose-Boyd RA, Li X (2022) Regulated degradation of HMG CoA reductase requires conformational changes in sterol-sensing domain. *Nat Commun* 13: 4273

Cho H, Stanzione F, Oak A, Kim GH, Yerneni S, Qi L, Sum AK, Chan C (2019) Intrinsic Structural Features of the Human IRE1alpha Transmembrane Domain Sense Membrane Lipid Saturation. *Cell Rep* 27: 307-320 e305

Christian AE, Haynes MP, Phillips MC, Rothblat GH (1997) Use of cyclodextrins for manipulating cellular cholesterol content. *Journal of Lipid Research* 38: 2264-2272

Christianson JC, Carvalho P (2022) Order through destruction: how ER-associated protein degradation contributes to organelle homeostasis. *The EMBO Journal* 41: e109845

Christianson JC, Jarosch E, Sommer T (2023) Mechanisms of substrate processing during ER-associated protein degradation. *Nat Rev Mol Cell Biol* 24: 777-796

Christianson JC, Olzmann JA, Shaler TA, Sowa ME, Bennett EJ, Richter CM, Tyler RE, Greenblatt EJ, Harper JW, Kopito RR (2011) Defining human ERAD networks through an integrative mapping strategy. *Nat Cell Biol* 14: 93-105

Chua NK, Hart-Smith G, Brown AJ (2019) Non-canonical ubiquitination of the cholesterol-regulated degron of squalene monooxygenase. *J Biol Chem* 294: 8134-8147

Chua NK, Howe V, Jatana N, Thukral L, Brown AJ (2017) A conserved degron containing an amphipathic helix regulates the cholesterol-mediated turnover of human squalene monooxygenase, a rate-limiting enzyme in cholesterol synthesis. *J Biol Chem* 292: 19959-19973

Cook ECL, Nelson JK, Sorrentino V, Koenis D, Moeton M, Scheij S, Ottenhoff R, Bleijlevens B, Loregger A, Zelcer N (2017) Identification of the ER-resident E3 ubiquitin ligase RNF145 as a novel LXR-regulated gene. *Plos One* 12: e0172721

Covino R, Ballweg S, Stordeur C, Michaelis JB, Puth K, Wernig F, Bahrami A, Ernst AM, Hummer G, Ernst R (2016) A Eukaryotic Sensor for Membrane Lipid Saturation. *Mol Cell* 63: 49-59

Cremer T, Jongsma MLM, Trulsson F, Vertegaal ACO, Neefjes J, Berlin I (2021) The ER-embedded UBE2J1/RNF26 ubiquitylation complex exerts spatiotemporal control over the endolysosomal pathway. *Cell reports* 34: 108659

Dawaliby R, Trubbia C, Delporte C, Noyon C, Ruysschaert JM, Van Antwerpen P, Govaerts C (2016) Phosphatidylethanolamine Is a Key Regulator of Membrane Fluidity in Eukaryotic Cells. *J Biol Chem* 291: 3658-3667

Elangovan M, Chong HK, Park JH, Yeo EJ, Yoo YJ (2017) The role of ubiquitin-conjugating enzyme Ube2j1 phosphorylation and its degradation by proteasome during endoplasmic stress recovery. *J Cell Commun Signal* 11: 265-273

Fenech EJ, Lari F, Charles PD, Fischer R, Laétitia-Thézénas M, Bagola K, Paton AW, Paton JC, Gyrd-Hansen M, Kessler BM *et al* (2020) Interaction mapping of endoplasmic reticulum ubiquitin ligases identifies modulators of innate immune signalling. *eLife* 9

Ferri-Blazquez A, Jarosch E, Sommer T (2023) Thioester and Oxyester Linkages in the Ubiquitin System. *Methods Mol Biol* 2602: 3-18

Foresti O, Rodriguez-Vaello V, Funaya C, Carvalho P (2014) Quality control of inner nuclear membrane proteins by the Asi complex. *Science* 346: 751-755

Frey S, Görlich D (2014) A new set of highly efficient, tag-cleaving proteases for purifying recombinant proteins. *Journal of Chromatography A* 1337: 95-105

Gautier R, Bacle A, Tiberti ML, Fuchs PF, Vanni S, Antonny B (2018) PackMem: A Versatile Tool to Compute and Visualize Interfacial Packing Defects in Lipid Bilayers. *Biophys J* 115: 436-444

Gill S, Stevenson J, Kristiana I, Brown AJ (2011) Cholesterol-dependent degradation of squalene monooxygenase, a control point in cholesterol synthesis beyond HMG-CoA reductase. *Cell Metab* 13: 260-273

Gotzke H, Kilisch M, Martinez-Carranza M, Sograte-Idrissi S, Rajavel A, Schlichthaerle T, Engels N, Jungmann R, Stenmark P, Opazo F *et al* (2019) The ALFA-tag is a highly versatile tool for nanobody-based bioscience applications. *Nat Commun* 10: 4403

Haider A, Wei Y-C, Lim K, Barbosa AD, Liu C-H, Weber U, Mlodzik M, Oras K, Collier S, Hussain MM *et al* (2018) PCYT1A Regulates Phosphatidylcholine Homeostasis from the Inner Nuclear Membrane in Response to Membrane Stored Curvature Elastic Stress. *Developmental Cell* 45: 481-495.e488

Heerklotz H (2008) Interactions of surfactants with lipid membranes. *Q Rev Biophys* 41: 205-264

Hernandez JM, Stein A, Behrmann E, Riedel D, Cypionka A, Farsi Z, Walla PJ, Raunser S, Jahn R (2012) Membrane fusion intermediates via directional and full assembly of the SNARE complex. *Science* 336: 1581-1584

Huang LJ, Chen RH (2023) Lipid saturation induces degradation of squalene epoxidase for sterol homeostasis and cell survival. *Life Sci Alliance* 6

Irisawa M, Inoue J, Ozawa N, Mori K, Sato R (2009) The sterol-sensing endoplasmic reticulum (ER) membrane protein TRC8 hampers ER to Golgi transport of sterol regulatory element-binding protein-2 (SREBP-2)/SREBP cleavage-activated protein and reduces SREBP-2 cleavage. *The Journal of Biological Chemistry* 284: 28995-29004

Jay AG, Hamilton JA (2017) Disorder Amidst Membrane Order: Standardizing Laurdan Generalized Polarization and Membrane Fluidity Terms. *J Fluoresc* 27: 243-249

Jiang L-Y, Jiang W, Tian N, Xiong Y-N, Liu J, Wei J, Wu K-Y, Luo J, Shi X-J, Song B-L (2018) Ring finger protein 145 (RNF145) is a ubiquitin ligase for sterol-induced degradation of HMG-CoA reductase. *The Journal of Biological Chemistry* 293: 4047-4055

Jo Y, Lee PCW, Sguigna PV, DeBose-Boyd RA (2011) Sterol-induced degradation of HMG CoA reductase depends on interplay of two Insigs and two ubiquitin ligases, gp78 and Trc8. *Proceedings of the National Academy of Sciences of the United States of America* 108: 20503-20508

Ju T, Bocik W, Majumdar A, Tolman JR (2010) Solution structure and dynamics of human ubiquitin conjugating enzyme Ube2g2. *Proteins* 78: 1291-1301

Jumper J, Evans R, Pritzel A, Green T, Figurnov M, Ronneberger O, Tunyasuvunakool K, Bates R, Zidek A, Potapenko A *et al* (2021) Highly accurate protein structure prediction with AlphaFold. *Nature* 596: 583-589

Kamel M, Lowe M, Schott-Verdugo S, Gohlke H, Kedrov A (2022) Unsaturated fatty acids augment protein transport via the SecA:SecYEG translocon. *FEBS J* 289: 140-162

Kapust RB, Tozser J, Fox JD, Anderson DE, Cherry S, Copeland TD, Waugh DS (2001) Tobacco etch virus protease: mechanism of autolysis and rational design of stable mutants with wild-type catalytic proficiency. *Protein Eng* 14: 993-1000

Karanasios E, Barbosa AD, Sembongi H, Mari M, Han G-S, Reggiori F, Carman GM, Siniossoglou S (2013) Regulation of lipid droplet and membrane biogenesis by the acidic tail of the phosphatidate phosphatase Pah1p. *Molecular Biology of the Cell* 24: 2124-2133

Keefe AD, Wilson DS, Seelig B, Szostak JW (2001) One-step purification of recombinant proteins using a nanomolar-affinity streptavidin-binding peptide, the SBP-Tag. *Protein expression and purification* 23: 440-446

Kelkar DA, Chattopadhyay A (2006) Membrane interfacial localization of aromatic amino acids and membrane protein function. *J Biosci* 31: 297-302

Khmelinskii A, Blaszczak E, Pantazopoulou M, Fischer B, Omnus DJ, Le Dez G, Brossard A, Gunnarsson A, Barry JD, Meurer M *et al* (2014) Protein quality control at the inner nuclear membrane. *Nature* 516: 410-413

Klemm EJ, Spooner E, Ploegh HL (2011) Dual role of ancient ubiquitous protein 1 (AUP1) in lipid droplet accumulation and endoplasmic reticulum (ER) protein quality control. *J Biol Chem* 286: 37602-37614

Kroon PC, Grunewald F, Barnoud J, van Tilburg M, Brasnett C, de Souza PCT, Wassenaar TA, Marrink S-JJ, 2025. Martinize2 and Vermouth: Unified Framework for Topology Generation. eLife Sciences Publications, Ltd.

Lee JP, Brauweiler A, Rudolph M, Hooper JE, Drabkin HA, Gemmill RM (2010) The TRC8 ubiquitin ligase is sterol regulated and interacts with lipid and protein biosynthetic pathways. *Molecular Cancer Research* 8: 93-106

Lee ME, DeLoache WC, Cervantes B, Dueber JE (2015) A Highly Characterized Yeast Toolkit for Modular, Multipart Assembly. *ACS Synth Biol* 4: 975-986

Lips C, Ritterhoff T, Weber A, Janowska MK, Mustroph M, Sommer T, Klevit RE (2020) Who with whom: functional coordination of E2 enzymes by RING E3 ligases during poly-ubiquitylation. *EMBO J* 39: e104863

Liu W, Shang Y, Zeng Y, Liu C, Li Y, Zhai L, Wang P, Lou J, Xu P, Ye Y *et al* (2014) Dimeric Ube2g2 simultaneously engages donor and acceptor ubiquitins to form Lys48-linked ubiquitin chains. *EMBO J* 33: 46-61

Manni MM, Tiberti ML, Pagnotta S, Barelli H, Gautier R, Antonny B (2018) Acyl chain asymmetry and polyunsaturation of brain phospholipids facilitate membrane vesiculation without leakage. *Elife* 7

Mehrtash AB, Hochstrasser M (2022) Elements of the ERAD ubiquitin ligase Doa10 regulating sequential poly-ubiquitylation of its targets. *iScience* 25: 105351

Menzies SA, Volkmar N, van den Boomen DJ, Timms RT, Dickson AS, Nathan JA, Lehner PJ (2018) The sterol-responsive RNF145 E3 ubiquitin ligase mediates the degradation of HMG-CoA reductase together with gp78 and Hrd1. *eLife* 7

Naughton FB, Alibay I, Barnoud J, Barreto-Ojeda E, Beckstein O, Bouysset C, Cohen O, Gowers RJ, MacDermott-Opeskin H, Matta M *et al* (2022) MDAnalysis 2.0 and beyond: fast and interoperable, community driven simulation analysis. *Biophysical Journal* 121: 272a-273a

Nilsson I, Ohvo-Rekila H, Slotte JP, Johnson AE, von Heijne G (2001) Inhibition of protein translocation across the endoplasmic reticulum membrane by sterols. *J Biol Chem* 276: 41748-41754

Okamoto M, Kurokawa K, Matsuura-Tokita K, Saito C, Hirata R, Nakano A (2012) High-curvature domains of the ER are important for the organization of ER exit sites in Saccharomyces cerevisiae. *Journal of Cell Science* 125: 3412-3420

Orlikowska-Rzeznik H, Krok E, Chattopadhyay M, Lester A, Piatkowski L (2023) Laurdan Discerns Lipid Membrane Hydration and Cholesterol Content. *J Phys Chem B* 127: 3382-3391

Pathre P, Shome K, Blumental-Perry A, Bielli A, Haney CJ, Alber S, Watkins SC, Romero G, Aridor M (2003) Activation of phospholipase D by the small GTPase Sar1p is required to support COPII assembly and ER export. *EMBO J* 22: 4059-4069

Pedersen KB, Ingólfsson HI, Ramirez-Echemendia DP, Borges-Araújo L, Andreasen MD, A CE-m, Melcr J, Ozturk TN, Bennett DWF, Kjølbye LR *et al* (2024) The Martini 3 Lipidome: Expanded and Refined Parameters Improve Lipid Phase Behavior. *ChemRviv*

Periole X, Cavalli M, Marrink SJ, Ceruso MA (2009) Combining an Elastic Network With a Coarse-Grained Molecular Force Field: Structure, Dynamics, and Intermolecular Recognition. *J Chem Theory Comput* 5: 2531-2543

Pierce NW, Kleiger G, Shan S-o, Deshaies RJ (2009) Detection of sequential polyubiquitylation on a millisecond timescale. *Nature* 462: 615-619

Pleiner T, Bates M, Trakhanov S, Lee C-T, Schliep JE, Chug H, Böhning M, Stark H, Urlaub H, Görlich D (2015) Nanobodies: site-specific labeling for super-resolution imaging, rapid epitope-mapping and native protein complex isolation. *eLife* 4: e11349

Popp MW, Antos JM, Ploegh HL (2009) Site-specific protein labeling via sortase-mediated transpeptidation. *Curr Protoc Protein Sci* Chapter 15: 15 13 11-15 13 19

Reinhard J, Starke L, Klose C, Haberkant P, Hammaren H, Stein F, Klein O, Berhorst C, Stumpf H, Saenz JP *et al* (2024) MemPrep, a new technology for isolating organellar membranes provides fingerprints of lipid bilayer stress. *EMBO J*

Renne MF, Ernst R (2023) Membrane homeostasis beyond fluidity: control of membrane compressibility. *Trends Biochem Sci* 48: 963-977

Ruggiano A, Mora G, Buxó L, Carvalho P (2016) Spatial control of lipid droplet proteins by the ERAD ubiquitin ligase Doa10. *The EMBO Journal* 35: 1644-1655

Sambrook J, Russell DW (2001) *Molecular cloning : a laboratory manual*. Cold Spring Harbor Laboratory Press, Cold Spring Harbor, N.Y.

Santinho A, Carpentier M, Lopes Sampaio J, Omrane M, Thiam AR (2024) Giant organelle vesicles to uncover intracellular membrane mechanics and plasticity. *Nat Commun* 15: 3767

Sarmento MJ, Llorente A, Petan T, Khnykin D, Popa I, Nikolac Perkovic M, Konjevod M, Jaganjac M (2023) The expanding organelle lipidomes: current knowledge and challenges. *Cell Mol Life Sci* 80: 237

Schägger H (2006) Tricine-SDS-PAGE. *Nature Protocols* 1: 16-22

Schindelin J, Arganda-Carreras I, Frise E, Kaynig V, Longair M, Pietzsch T, Preibisch S, Rueden C, Saalfeld S, Schmid B *et al* (2012) Fiji: an open-source platform for biological-image analysis. *Nature Methods* 9: 676-682

Schmidt CC, Vasic V, Stein A (2020) Doa10 is a membrane protein retrotranslocase in ER-associated protein degradation. *Elife* 9

Schumacher MM, DeBose-Boyd RA (2021) Posttranslational Regulation of HMG CoA Reductase, the Rate-Limiting Enzyme in Synthesis of Cholesterol. *Annual Review of Biochemistry* 90: 659-679

Sharpe HJ, Stevens TJ, Munro S (2010) A comprehensive comparison of transmembrane domains reveals organelle-specific properties. *Cell* 142: 158-169

Sharpe LJ, Howe V, Scott NA, Luu W, Phan L, Berk JM, Hochstrasser M, Brown AJ (2019) Cholesterol increases protein levels of the E3 ligase MARCH6 and thereby stimulates protein degradation. *The Journal of Biological Chemistry* 294: 2436-2448

Shen Y, Zhao Z, Zhang L, Shi L, Shahriar S, Chan RB, Di Paolo G, Min W (2017) Metabolic activity induces membrane phase separation in endoplasmic reticulum. *Proc Natl Acad Sci U S A* 114: 13394-13399

Sheng Y, Hong JH, Doherty R, Srikumar T, Shloush J, Avvakumov GV, Walker JR, Xue S, Neculai D, Wan JW *et al* (2012) A human ubiquitin conjugating enzyme (E2)-HECT E3 ligase structure-function screen. *Mol Cell Proteomics* 11: 329-341

Souza PCT, Alessandri R, Barnoud J, Thallmair S, Faustino I, Grunewald F, Patmanidis I, Abdizadeh H, Bruininks BMH, Wassenaar TA *et al* (2021) Martini 3: a general purpose force field for coarse-grained molecular dynamics. *Nat Methods* 18: 382-388

Spandl J, Lohmann D, Kuerschner L, Moessinger C, Thiele C (2011) Ancient ubiquitous protein 1 (AUP1) localizes to lipid droplets and binds the E2 ubiquitin conjugase G2 (Ube2g2) via its G2 binding region. *The Journal of Biological Chemistry* 286: 5599-5606

Stefanovic-Barrett S, Dickson AS, Burr SP, Williamson JC, Lobb IT, van den Boomen DJ, Lehner PJ, Nathan JA (2018) MARCH6 and TRC8 facilitate the quality control of cytosolic and tail-anchored proteins. *EMBO Rep* 19

Stein A, Radhakrishnan A, Riedel D, Fasshauer D, Jahn R (2007) Synaptotagmin activates membrane fusion through a Ca2+-dependent trans interaction with phospholipids. *Nat Struct Mol Biol* 14: 904-911

Stein A, Ruggiano A, Carvalho P, Rapoport TA (2014) Key steps in ERAD of luminal ER proteins reconstituted with purified components. *Cell* 158: 1375-1388

Stevenson J, Huang EY, Olzmann JA (2016) Endoplasmic Reticulum-Associated Degradation and Lipid Homeostasis. *Annual review of nutrition* 36: 511-542

Stevenson J, Luu W, Kristiana I, Brown AJ (2014) Squalene mono-oxygenase, a key enzyme in cholesterol synthesis, is stabilized by unsaturated fatty acids. *Biochem J* 461: 435-442

Swarnkar A, Leidner F, Rout AK, Ainatzi S, Schmidt CC, Becker S, Urlaub H, Griesinger C, Grubmuller H, Stein A (2024) Determinants of chemoselectivity in ubiquitination by the J2 family of ubiquitin-conjugating enzymes. *EMBO J* 43: 6705-6739

Tan JME, Cook ECL, van den Berg M, Scheij S, Zelcer N, Loregger A (2019) Differential use of E2 ubiquitin conjugating enzymes for regulated degradation of the rate-limiting enzymes HMGCR and SQLE in cholesterol biosynthesis. *Atherosclerosis* 281: 137-142

van de Weijer ML, Schuren ABC, van den Boomen DJH, Mulder A, Claas FHJ, Lehner PJ, Lebbink RJ, Wiertz E (2017a) Multiple E2 ubiquitin-conjugating enzymes regulate human cytomegalovirus US2-mediated immunoreceptor downregulation. *J Cell Sci* 130: 2883-2892

van de Weijer ML, Schuren ABC, van den Boomen DJH, Mulder A, Claas FHJ, Lehner PJ, Lebbink RJ, Wiertz EJHJ (2017b) Multiple E2 ubiquitin-conjugating enzymes regulate human cytomegalovirus US2-mediated immunoreceptor downregulation. *Journal of Cell Science* 130: 2883-2892

van der Does C, Swaving J, van Klompenburg W, Driessen AJ (2000) Non-bilayer lipids stimulate the activity of the reconstituted bacterial protein translocase. *J Biol Chem* 275: 2472-2478

Vera Rodriguez A, Frey S, Gorlich D (2019) Engineered SUMO/protease system identifies Pdr6 as a bidirectional nuclear transport receptor. *J Cell Biol* 218: 2006-2020

Volkmar N, Gawden-Bone CM, Williamson JC, Nixon-Abell J, West JA, St George-Hyslop PH, Kaser A, Lehner PJ (2022) Regulation of membrane fluidity by RNF145-triggered degradation of the lipid hydrolase ADIPOR2. *The EMBO Journal* 41: e110777

Volmer R, van der Ploeg K, Ron D (2013) Membrane lipid saturation activates endoplasmic reticulum unfolded protein response transducers through their transmembrane domains. *Proc Natl Acad Sci U S A* 110: 4628-4633

Wang L, Brasnett C, Borges-Araujo L, Souza PCT, Marrink SJ (2025) Martini3-IDP: improved Martini 3 force field for disordered proteins. *Nat Commun* 16: 2874

Wang X, Herr RA, Rabelink M, Hoeben RC, Wiertz EJ, Hansen TH (2009) Ube2j2 ubiquitinates hydroxylated amino acids on ER-associated degradation substrates. *J Cell Biol* 187: 655-668

Weber A, Cohen I, Popp O, Dittmar G, Reiss Y, Sommer T, Ravid T, Jarosch E (2016) Sequential Poly-ubiquitylation by Specialized Conjugating Enzymes Expands the Versatility of a Quality Control Ubiquitin Ligase. *Molecular Cell* 63: 827-839

Weigel AV, Chang CL, Shtengel G, Xu CS, Hoffman DP, Freeman M, Iyer N, Aaron J, Khuon S, Bogovic J *et al* (2021) ER-to-Golgi protein delivery through an interwoven, tubular network extending from ER. *Cell* 184: 2412-2429 e2416

Wilkins MR, Gasteiger E, Bairoch A, Sanchez JC, Williams KL, Appel RD, Hochstrasser DF (1999) Protein identification and analysis tools in the ExPASy server. *Methods Mol Biol* 112: 531-552

Yan R, Cao P, Song W, Li Y, Wang T, Qian H, Yan C, Yan N (2021a) Structural basis for sterol sensing by Scap and Insig. *Cell Rep* 35: 109299

Yan R, Cao P, Song W, Qian H, Du X, Coates HW, Zhao X, Li Y, Gao S, Gong X *et al* (2021b) A structure of human Scap bound to Insig-2 suggests how their interaction is regulated by sterols. *Science* 371

Yoshioka H, Coates HW, Chua NK, Hashimoto Y, Brown AJ, Ohgane K (2020) A key mammalian cholesterol synthesis enzyme, squalene monooxygenase, is allosterically stabilized by its substrate. *Proc Natl Acad Sci U S A* 117: 7150-7158

Zelcer N, Sharpe LJ, Loregger A, Kristiana I, Cook EC, Phan L, Stevenson J, Brown AJ (2014) The E3 ubiquitin ligase MARCH6 degrades squalene monooxygenase and affects 3-hydroxy-3-methyl-glutaryl coenzyme A reductase and the cholesterol synthesis pathway. *Mol Cell Biol* 34: 1262-1270

Zhou Z, Torres M, Sha H, Halbrook CJ, Van den Bergh F, Reinert RB, Yamada T, Wang S, Luo Y, Hunter AH *et al* (2020) Endoplasmic reticulum-associated degradation regulates mitochondrial dynamics in brown adipocytes. *Science* 368: 54-60

Figure Legends

Figure 1: E2 enzymatic activity is low in ER-like membranes

(**A**) Schematic of ubiquitin loading assay. Fluorescently labeled E2s were incubated at 37 ^{o}C with ubiquitin-loaded E1 Uba1 in the presence of ATP and free ubiquitin. UBE2J1 and UBE2J2 both possess an N-terminal UBC domain connected to the C-terminal transmembrane segment by a disordered region. The red star marks the position of the fluorescent label. (**B**) UBE2J2$_{DL680}$, reconstituted into ER-like liposomes (protein: lipid ratio 1:32,000) or dissolved in detergent, was subjected to the reaction described in (A). Samples were collected at indicated time points, separated by non-reducing SDS-PAGE, and analyzed by fluorescence scanning. Where indicated, ATP was omitted (-ATP) or the 10 min sample was reduced with 2% (v/v) 2-mercaptoethanol (R). (**C**) Quantification of ubiquitin-loaded UBE2J2$_{DL680}$ from reactions as in (B). Lines connect mean values. For reactions with more than three replicates, error bars indicate the mean ± standard deviation (n=7, detergent; n=3, ER-like liposomes) (**D**) Ubiquitin loading assay as in (B), but with UBE2J1$_{DL680}$. (**E**) Quantification of ubiquitin-loaded UBE2J1$_{DL680}$ from reactions as in (D) (n=3, both conditions). R= reduced. ER-like liposomes contained 60 mol% POPC, 20 mol% DOPE, 10 mol% DOPS, 10 mol% cholesterol. Complete lipid compositions are given in Table 6.

Figure 2: Membrane composition dictates the efficiency of thiol-ester bond formation

(**A**) Ubiquitin loading assay (as in Fig. 1A), with UBE2J2$_{DL680}$ reconstituted into liposomes containing of 80 mol% PC and 20 mol% PE with indicated saturated fatty acids (SFA) content. (**B**) Quantification of assays as in (A); n=7 (10% SFAs), n=8 (60% SFAs), n=3 (50% SFAs). Solid lines connect mean values; for n>3, error bars represent mean ± s.d., standard deviation (**C**) As in (A), but with liposomes varying in di-unsaturated lipid content (P/L= 1: 32,000). (**D**) Quantification of reactions as in (C). n=3 (50% SFAs), n=4 (40% and 35% SFAs). (**E**) Lipid packing of protein- and sterol-free liposomes with various SFA contents measured by C-Laurdan fluorescence. Emission spectra were recorded at 37°C (n≥3); generalized polarization was calculated as described (Ballweg *et al.*, 2020). (**F**) Ubiquitin loading of UBE2J2$_{DL680}$, reconstituted in PC-only liposomes with indicated SFA content (P/L= 1: 32,000). (**G**) Quantification of reactions as in (F). Data for PC-only liposomes are shown in blue and green (n=3); for comparison, data from (B) obtained with PC/PE liposomes are shown black and red. (**H**) Ubiquitin loading of UBE2J2$_{DL680}$, reconstituted in PC/PE liposomes with indicated SFA content with or without 10 mol% cholesterol (P/L= 1: 32,000). (**I**) Quantification of reactions as in (H). Mean values are connected by solid lines;

n=2 (35% SFAs ± cholesterol, n=6 (60% SFAs, no cholesterol), n=3 (60% SFAs + 10% cholesterol). For n>3, error bars represent mean ± s.d. Detailed liposome compositions are given in Table 6.

Figure 3: Lipid packing affects UBE2J2 conformation

(**A**) Limited proteolysis assay of UBE2J2DL680 reconstituted into liposomes with indicated SFA content (P/L= 1: 32,000), incubated with increasing trypsin concentrations (0, 1.9, 5.6, 16.6 or 50 ng/µl) at 25 °C for 30 min. Schematic (left) shows predicted tryptic sites (100% cleavage probability, PeptideCutter (Wilkins *et al*, 1999); the red star indicates the position of the fluorescent label. Reaction products were analyzed by SDS-PAGE and fluorescence scanning. (**B**) Distribution of $UBE2J2_{DL680}$ fluorescence along the gel lane for proteoliposomes incubated with 1.85 ng/µl trypsin from (A). (**C**) Fluorescence emission spectra of liposomes reconstituted with the FRET donor $UBE2J2_{A488}$ in the absence or presence of the FRET acceptor $UBE2J2_{A594}$ (P/L = 1:20,000 and 1:5000, respectively). Each condition overlays six curves (two reconstitutions, each measured in triplicate). Data were normalized to the emission at 516 nm. (**D**) Relative FRET efficiency calculated from spectra in (C) as the ratio of acceptor to donor emission intensity (I_{614}/I_{516}). (**E**) Cysteine crosslinking of $UBE2J2_{DL680}$ in liposomes with the indicated SFA content (P/L = 1:32,000), incubated with the indicated concentrations of 1,4-bismaleimidobutane (BMB) or 1,2-bismaleimidoethane (BMOE). Samples were analyzed by SDS-PAGE and fluorescence scanning. (**F**) Ubiquitin loading of $UBE2J2_{DL680}$, reconstituted in liposomes with 10% SFA content (P/L = 1:32,000), and the indicated proteins at different protein to lipid ratio (P/L). (**G**) Quantification of reactions in (F). Detailed liposome compositions are given in Table 6.

Figure 4: E1 enzyme interaction is impaired in membranes with lipid packing defects

(**A**) Ubiquitin loading of UBE2J2 chimeras with UBE2J1 TMS and/or disordered linker, reconstituted in PC/PE liposomes with the indicated saturated fatty acids (SFA) content. (**B**) Quantification of reactions as in (A) (n=2). *co-purified UBE2J2 fragment. (**C**) Ubiquitin loading of $UBE2J2_{DL680}$, reconstituted in liposomes with 10% SFAs, pre-incubated with the indicated n-octyl-β-D-glucoside (OG) concentrations for 10 minutes prior to ubiquitin loading reaction. Samples collected at indicated time points were analyzed by non-reducing SDS-PAGE and fluorescence scanning. ATP was omitted where indicated (-ATP). (**D**) Quantification of (C). (**E**) Limited proteolysis assay on liposomes containing $UBE2J2_{DL680}$. $UBE2J2_{DL680}$ was reconstituted in liposomes as described in (C). Proteoliposomes were pre-incubated with the indicated concentrations of *n*-octyl-β-D-glucoside (OG) for 10 minutes

prior to trypsinization for 30 minutes at 37 °C (0, 1.9, 5.6 or 16.6 ng/µl trypsin). Samples were analyzed by SDS-PAGE and fluorescence scanning. (**F**) Linegraph showing the probability of contacts between the UBC domain and the ER membrane. The probability distribution can be described by a four component Poisson mixture model, that separates the unbound, loosely bound (with a mean of 8 contacts), and two tightly bound conformations (30 and 50 contacts, respectively). Representative structures for the first three components are shown in panels above the plot. (**G**) Lineplot showing contact frequency between the UBC domain and the different membranes (blue for ER-like, green and yellow for 10% and 60% SFA content, respectively). **(H)** Contact frequency for the ER-like membrane in (G) mapped onto the structure of UBE2J2. (**I**) Ubiquitin loading of wild type (WT) and mutant (F137E) UBE2J2, reconstituted in liposomes composed of 80 mol% PC and 20 mol% PE with the indicated content of SFAs. (**J**) Quantification of reactions as in (F) (n=3 for F137E, n=7 for WT in 10% SFAs, n=8 in 60% SFAs). (**K**) Cysteine crosslinking for analysis of UBE2J2:E1 interaction. $UBE2J2_{DL680}$ liposomes with the indicated SFA content were incubated with the E1 Uba1 in the presence or absence of 1,2-bismaleimidoethane (BMOE) crosslinker. In detergent-containing reactions, proteoliposomes were pre-incubated with OG for 10 minutes prior to addition of the crosslinker. Samples collected at the indicated time points were analyzed by SDS-PAGE and fluorescence scanning. UBE2J2 was reconstituted at a protein to lipid ratio of 1/32,000. Detailed liposome compositions are given in Table 6.

Figure 5: UBE2J2 activity modulates ubiquitination cascade outcome

(**A**) Ubiquitination of RNF145 and UBE2J2. Fluorescently labeled proteins were co-reconstituted in PC/PE liposomes with the indicated saturated fatty acids (SFA) content (Protein to lipid ratios (P/L): ^{DL800}RNF145-ALFA/L, 1:32,000; $UBE2J2_{DL680}$, 1:32,000). Samples collected at indicated time points were analyzed by reducing SDS-PAGE and fluorescence scanning. (**B**, **C**) Quantification of ubiquitinated RNF145 (B, n=10) and UBE2J2 (C, n≥6) from reactions as in (A). Solid lines connect mean values, error bars indicate the mean ± standard deviation (s.d.). (**D**) Quantification of RNF145-ALFA ubiquitination with soluble UBE2J2 ($sUBE2J2_{1-226}$). ^{DL800}RNF145-ALFA was reconstituted in liposomes with indicated SFA content (P/L = 1:32,000) and incubated with E1, ubiquitin, ATP and 0.5 µM $sUBE2J2_{1-226}$. Samples were analyzed as above (n=2). (**E**) Ubiquitination of SQLE by MARCHF6 and UBE2J2. ^{DL800}SQLE, MARCHF6 and $UBE2J2_{DL680}$ were co-reconstituted in PC/PE liposomes with the indicated SFA content and P/L = 1:32,000 for each protein. Samples collected at the indicated time points were analyzed by reducing SDS-PAGE and fluorescence scanning. Samples were analyzed as above. (**F**) Quantification of ubiquitinated SQLE from reactions as in (E) (n=2). (**G**) Quantification of SQLE ubiquitination by

MARCHF6 and soluble UBE2J2. ^{DL800}SQLE and MARCHF6 were co-reconstituted in PC/PE liposomes with the indicated SFA content, P/L = 1:16,000 for each protein. sUBE2J2 was added at indicated concentrations. (**H**) Analysis of the RNF145–UBE2J2 interaction. ^{DL800}RNF145-ALFA, UBE2J2$_{DL680}$ and Syb2$_{A488}$ were co-reconstituted in liposomes with indicated SFA content, each at P/L = 1:32,000. Immunoprecipitation was performed with a biotinylated anti-ALFA nanobody, eluted using SUMO protease Ulp1*. Co-reconstitution was estimated from immunoprecipitation of intact liposomes; Protein interactions were assessed by immunoprecipitation RNF145-ALFA from detergent-solubilized liposomes. (**I**) Quantification of UBE2J2$_{DL680}$ co-purifying with RNF145-ALFA from solubilized liposomes in (H). The fraction of eluted UBE2J2$_{DL680}$ was normalized to eluted RNF145-ALFA and to the UBE2J2$_{DL680}$ input (n=6). Error bars represent mean ± s.d. Statistical significance was assessed using a paired sample t-test (* p = 0.00283). Detailed liposome compositions are given in Table 6.

Figure 6: Cholesterol modulates auto-regulation of the E3 ubiquitin ligase RNF145

(**A**) Ubiquitination of RNF145 with a soluble UBE2J2 (sUBE2J2$_{1-226}$). Fluorescently labeled ^{DL800}RNF145-ALFA was reconstituted in ER-like liposomes with or without 10 mol% cholesterol (P/L = 1:32,000) and was incubated with E1, ubiquitin, ATP and 2 μM sUBE2J2$_{1-226}$. Samples were analyzed by reducing SDS-PAGE and fluorescence scanning at indicated time points. (**B**) Quantification of ubiquitinated RNF145 from (A) (n=3). Statistical significance was assessed using Welch's two-sample t-test for each time point: * p=0.02561, ** p=0.00057, *** p=0.03553, **** p=0.06854 (n.s.) (**C**) Ubiquitination of RNF145 with UBE2J2. Proteins were co-reconstituted in liposomes with 60% SFA content, with or without 10mol% cholesterol (P/L = 1: 32,000 for both proteins). Samples were analyzed as above. (**D**) Quantification of ubiquitinated RNF145 from (C), n=3 (with cholesterol), n=10 (without cholesterol). Error bars indicate the mean ± standard deviation. Statistical significance was assessed using Welch's two-sample t-test for each time point: * p=0.000134, ** p=0.00071, *** p=0.00011, **** p=0.000024 (**E**) Analysis of RNF145 oligomerization. ^{DL800}RNF145-ALFA was co-reconstituted with Syb2$_{A488}$ and RNF145$_{\Delta RING}$-sfGFP (the C-terminal cytoplasmic part including the RING domain was replaced with superfolder GFP) in (liposomes of indicated SFA content ± 10% cholesterol (P/L= 1:32,000). After solubilization, proteins were precipitated with anti-GFP or anti-ALFA nanobodies. Samples were analyzed by SDS-PAGE and fluorescence scanning. (**F**) Quantification of co-purified RNF145 upon immunoprecipitation of RNF145-ALFA or RNF145$_{\Delta RING}$-sfGFP from the experiment in (E). The co-purifying RNF145 variant was normalized to nanobody-precipitated RNF145 and to the input. Detailed liposome compositions are given in Table 6.

Figure 7: Model for regulation of the ubiquitination cascade by membrane composition

UBE2J2 adopts different conformations dependent on membrane environment, thereby controlling its activity. Hydrophobic interactions between the cytosolic region of UBE2J2 and the membrane stabilize an auto-inhibited conformation. In the active state (left), the cytosolic region is accessible for E1-mediated loading. membranes enriched in unsaturated lipids, exhibit packing defects (top), stabilizing an inactive UBE2J2 conformation that impairs interaction with the E1 and E3 enzymes. Increasing local UBE2J2 concentration overrides this inhibition via dimerization, promoting interaction with RNF145 and E3 activity (middle). Increasing lipid saturation enhances lipid packing and favors an active UBE2J2 conformation. Ubiquitin loading of UBE2J2 and physical interaction with its cognate E3s, including RNF145, is enhanced (bottom). RNF145 is directly regulated by cholesterol, which might promote its oligomerization and auto-ubiquitination (right).

Extended Data Figure 1 - Purification and characterization of UBE2J1/2 and assay controls (related to Fig. 1)

(**A, B**) Purified, fluorescently labelled UBE2J2 (A) and UBE2J1 (B) were analyzed by SDS-PAGE and visualized by Coomassie staining or fluorescence scanning. Size exclusion chromatography performed on a Superdex 200 10/300 GL column, shows major elution peaks for UBE2J2 and UBE2J1 (brackets) and later peaks for free fluorescent peptide. (**C**) Flotation assay on a 0-40% (w/v) Nycodenz gradient assessing UBE2J2 reconstitution in liposomes of ER-like composition. The fractionated gradient analyzed by SDS-PAGE and fluorescence scanning demonstrates UBE2J2 migrates with liposomes to top fractions. (**D**) Extended time course of ubiquitin loading and auto-ubiquitination of $UBE2J2_{DL680}$ reconstituted in ER-like liposomes (P/L= 1: 32,000). (**E**) Quantification of (D, n=3) (**F**) Ubiquitin loading of WT, C94 only (C33S/C88S/C157S) or C94A $UBE2J2_{DL680}$ in 0.03% (w/v) DDM. (**G**) Quantification of (F, n=2). (**H**) Analysis of UBE2J2 orientation in ER-like liposomes (P/L= 1:32,000) assessed by antibody-mediated quenching of AlexaFluor 488 fluorescence. Correctly-oriented $UBE2J2_{A488}$ is protected from antibody-mediated quenching (64 ± 2 % at t = 200 s); solubilization with 1% Triton-X100allows quenching. Reactions in 0.03% (w/v) DDM serve as a positive control (n=3 for detergent, n=2 for ER-like liposomes, including 2 technical replicates for each). Bands represent the mean and error from all replicates. (**I**) Analysis of UBE2J2 orientation in ER-like liposomes (P/L= 1;32,000) by protease protection. Quantification of Ulp1-mediated cleavage of His14-SUMO-$UBE2J2_{DL680}$ reconstituted in ER-like liposomes indicates 95% correct orientation. Ulp1 cleaves the N-terminal SUMO tag of correctly-oriented UBE2J2 (n=3). (**J**) Loading of the E1 Uba1 with fluorescently labeled ubiquitin in the presence of protein-free ER-like liposomes at indicated lipid concentrations; analyzed by non-reducing SDS-PAGE and fluorescence scanning. (**K**) Effect of increasing E1 concentration on ubiquitin loading of $UBE2J2_{DL680}$ in ER-like liposomes; analyzed by non-

reducing SDS-PAGE and fluorescence scanning. (**L**) Ubiquitin loading of $UBE2J2_{DL680}$ in detergent-solubilized liposomes. $UBE2J2_{DL680}$ was reconstituted in ER-like liposomes (P/L= 1:32,000). Prior to ubiquitin loading, liposomes were solubilized with n-decyl-β-D-maltoside (DM) or Triton X-100 at the indicated concentrations; analyzed by non-reducing SDS-PAGE and fluorescence scanning. (**M**) Quantification (L). Graph contains data from Figure 1C for comparison. (**N**) As in (H), for $UBE2J1_{A488}$. R=reduced. a.u. = arbitrary units. ER-like liposomes contained 60 mol% POPC, 20 mol% DOPE, 10 mol% DOPS, 10 mol% cholesterol.

Extended Data Figure 2 - UBE2J2/1 reconstitution and activity in liposomes of defined acyl chain composition (related to Fig. 2)

(**A**) Flotation assay to assess UBE2J2 reconstitution in liposomes with lipid compositions as in Fig. 2. UBE2J2 migrates with liposomes to the top fractions of a 0-40% (w/v) Nycodenz density gradient; gradient fractions analyzed by SDS-PAGE and fluorescence scanning. (**B**) Orientation analysis of UBE2J2 in liposomes with 10% or 60% SFAs (P/L= 1: 32,000), assessed by antibody-mediated quenching of AlexaFluor 488 fluorescence. Correct orientation protects from quenching; solubilization with 1% Triton-X100 leads to quenching of also correctly oriented $UBE2J2_{A488}$. Antibody-mediated quenching of $UBE2J2_{A488}$ fluorescence in 0.03% (w/v) DDM solution was used as a positive control (n=2 for each, including technical replicates for each). Bands represent the error and mean of technical replicates. (**C**) Effect of E1 concentration on ubiquitin loading of $UBE2J2_{DL680}$ reconstituted in liposomes with 50% SFA content; analyzed by non-reducing SDS-PAGE and fluorescence scanning. (**D**) Ubiquitin loading of $UBE2J2_{DL680}$ in liposomes containing 10% SFA with indicated acyl chain lengths (P/L= 1:32,000). In comparison to the standard 10% SFA liposomes, di-oleyl-PC (18:1) was replaced with 1,2-dipalmitoleoyl-PC (16:1). (**E**) Quantification of (D, n=3). Graph contains data from Fig. 2B for comparison. (**F**) Kinetic analysis of ubiquitin loading of UBE2J2 by quenched-flow. Equal volumes of reaction solution A, containing $UBE2J2_{DL680}$ in liposomes with 10% or 60% SFAs, and reaction solution B (E1, ubiquitin and ATP) were rapidly mixed; quenched with 0.1 M HCl; analyzed by SDS-PAGE and fluorescence scanning. Data from Fig. 2B is included in the plot and used for the fitting procedure. The table shows the results of the fitting procedure with units s^{-1}. (**G**) Discharge kinetics of ubiquitin-loaded UBE2J2, reconstituted in liposomes with 10% or 60% SFAs (P/L=1:32,000). $UBE2J2_{DL680}$ was loaded (10 min for 10% SFAs, 1 min for 60% SFAs, 50 nM UBE2J2, 20 nM E1), diluted 10-fold, and discharge monitored in quench buffer with EDTA and 2 µM Rad6 to minimize residual E1. (**H**) Quantification of the loaded UBE2J2 fraction in (G). Data were normalized to timepoint 0. (**I**) Ubiquitin loading of $UBE2J1_{DL680}$, in liposomes with the indicated SFA content. (**J**) Quantification of reactions as

in (H) (n=2). (**K**) As in (B), for UBE2J1 (n=2 technical replicates). (**L**) The effect of cholesterol on the lipid packing in liposomes assessed by C-Laurdan fluorescence; emission spectra were recorded at 37°C and generalized polarization calculated as described (Ballweg *et al.*, 2020) (n≥3). (**M, N**) Dynamic light scattering analysis of protein-free (M) and UBE2J2-containing (N) liposomes with indicated lipid compositions and protein/lipid ratios. Bars represent mean ± s.d. or triplicates (M), or the mean of multiple technical replicates. (**O**) The effect of proteins on the lipid packing of liposomes with variable lipid acyl chain saturation and cholesterol content assessed with C-Laurdan fluorescence as in (L), but comparing protein-free with UBE2J2 liposomes (n≥3). Unless indicated otherwise, E2s were reconstituted at a P/L of 1/32,000. R = reduced. Detailed liposome compositions are given in Table 6.

Extended Data Figure 3 - UBE2J2 reconstitution, structural analysis, and assay (related to Fig. 3)

(**A**) Limited proteolysis of $UBE2J2_{DL680}$ reconstituted in liposomes with indicated SFA content (P/L = 1:32,000). Liposomes were treated with increasing trypsin concentrations (0, 1.9, 5.6 or 16.6 ng/µl) at 25 °C for 30 minutes Samples were analyzed by SDS-PAGE and fluorescence scanning. (**B**) Specificity of acceptor emission in FRET experiments (see Fig. 3C, D). Liposomes were reconstituted with $UBE2J2_{A488}$ (donor), $UBE2J2_{A594}$ (acceptor), or both (P/L = 1:20,000 and 1:5000 for $UBE2J2_{A488}$ and $UBE2J2_{A594}$, respectively; emission at 614 nm (excitation 480 nm) was measured at 25°C. Data represent two independent reconstitutions, each measured in triplicate (n=2). (**C**) Cysteine crosslinking of $UBE2J2_{DL680}$ in liposomes (P/L = 1:32,000 or 1:4000) using 20 µM BMOE for 30 min at 25°C. Products analyzed by SDS–PAGE and fluorescence scanning. (**D**) Purified soluble UBE2J2 ($sUBE2J2_{1-226}$) analyzed by SDS-PAGE and Coomassie staining. SEC of $sUBE2J2_{1-226}$ was performed with a HiLoad S75 16/60 column. Brackets indicate the elution peak of soluble UBE2J2. (**E**) Ubiquitin loading of $sUBE2J2_{1-226}$ analyzed by SDS-PAGE and stain-free scanning. R= reduced with β-mercaptoethanol. (**F**) Crosslinking of $sUBE2J2_{1-226}$ with 2 mM BMOE for 30 min at 25°C, analyzed by SDS–PAGE and stain-free scanning. (**G**) Limited proteolysis of $UBE2J2_{DL680}$ reconstituted in liposomes with indicated SFA content as in (A), but with P/L = 1:4000 or 1:1000. Detailed liposome compositions are given in Table 6.

Extended Data Figure 4 - Characterization of UBE2J2/1 chimeras and sensitivity to membrane composition (related to Fig. 4)

(**A**) Loading of $sUBE2J2_{1-226}$ with fluorescent ubiquitin in the presence of protein-free liposomes. (**B**) Purified, fluorescently labelled UBE2J2 chimeras with the disordered linker or the transmembrane segment (TMS) of UBE2J1 or the TMS of Syb2, analyzed by SDS-PAGE

and Coomassie staining. Size-exclusion chromatography (SEC, Superdex 200 10/300 GL) shows elution peaks for chimeras (brackets). (**C**) Quantification of ubiquitin loading of UBE2J2 with the TMS of Syb2, reconstituted in PC/PE liposomes with the indicated saturated fatty acid (SFA) content (n=2). (**D**) Purified, fluorescently labelled UBE2J1 chimeras with the disordered linker or the TMS of UBE2J2, analyzed by SDS-PAGE and Coomassie staining or fluorescence scanning. SEC (Superdex 200 10/300 GL) shows elution peaks for chimeras (brackets); late peak indicates free fluorescent peptide. (**E**) Ubiquitin loading of UBE2J1 chimeras bearing the TMS or disordered linker of UBE2J2, reconstituted in PC/PE liposomes with the indicated SFA content. Asterisk indicates a contaminating protein. (**F**) Quantification of reactions (E) (n=2). (**G**) Solubilization of protein-free liposomes upon addition of increasing *n*-octyl-β-D-glucoside (OG) concentrations measured by loss of light scattering. (**H**) Effect of OG on lipid packing in liposomes with 10% SFA content assessed with C-Laurdan fluorescence; emission spectra recorded at 25 °C, before and after the OG addition (n=2). Generalized polarization calculated as described (Ballweg *et al.*, 2020). (**I**) Ubiquitin loading of $UBE2J2_{DL680}$ reconstituted in liposomes (60% SFAs, P/L= 1;32,000) after incubation with the indicated OG concentrations for 10 min. Detailed liposome compositions are given in Table 6.

Extended Data Figure 5 – Molecular dynamics simulations and characterization of the F137E mutant (related to Fig. 4)

(**A**) Bar graph of membrane packing defect sizes for different lipid compositions. The packing defect constant (□) relates to the probability p(A) of finding a lipid packing defect in an area A, described by $p(A) = b \times e^{-\frac{A}{\pi}}$. The packing defect constant represents the probability of encountering larger packing defects. PackMem was used to calculate and group membrane defects (Gautier *et al.*, 2018). (**B**) Probability of UBE2J2 adopting one of the membrane-bound versus unbound conformations in membranes of different lipid compositions, as determined by molecular dynamics simulations. (**C**) Ubiquitin loading of WT, F137Y or F100A $UBE2J2_{DL680}$, reconstituted in liposomes with 10% SFA content (P/L= 1:32,000; n=7 for WT, n=3 for F137Y, n=2 for F100A). (**D**) Limited proteolysis assay on WT or F137E $UBE2J2_{DL680}$ reconstituted in liposomes with indicated SFA content (P/L = 1:32,000) using increasing trypsin concentrations (0, 1.9, 5.6 or 16.6 ng/µl) at 25 °C for 30 min; analyzed by SDS-PAGE and fluorescence scanning. (**E**) Cysteine crosslinking to assess interaction of UBE2J2 (WT, F137Y, or F137E) with E1 in liposomes with the 10% SFA content, in the presence or absence of 1,2-bismaleimidoethane (BMOE). Samples collected after 10 minutes, analyzed by SDS-PAGE and fluorescence scanning (OE= overexposed). UBE2J2 was reconstituted at P/L = 1:32,000. Detailed liposome compositions are given in Table 6.

Extended Data Fig. 6 - Characterization and activity of E3 ubiquitin ligases and partners in reconstituted systems (related to Fig. 5).

(**A**-**C**) Purified, fluorescently labelled E3 ubiquitin ligases RNF145-ALFA (A), RNF139-ALFA (B), and MARCH6-TEV-SBP (C), analyzed by SDS-PAGE with Coomassie staining or fluorescence scanning. Size-exclusion chromatography (Superose 6 10/300 GL) shows elution peaks (brackets) of E3s. (**D**) Flotation assay assessing E3 reconstitution in liposomes with varying SFA content. E3s co-migrate with liposomes to top fractions of a 0-40% (w/v) Nycodenz gradient; gradient fractions analyzed by SDS-PAGE and fluorescence scanning. (**E**) Protease protection assay for E3 orientation. RNF145-TEV-SBP was reconstituted in liposomes with indicated lipid compositions and treated with TEV protease (± 0.8 (w/v) % Triton X-100), followed by SDS–PAGE and anti-SBP western blotting. Numbers below the Western blot images indicate the fraction of signal remaining after the indicated treatments. (**F**) Purified UBE2G2 analyzed by SDS–PAGE and Coomassie staining; size-exclusion chromatography (HiLoad S75 16/60) with elution peak indicated (bracket). (**G**) Purified TM_{Cue1}-$AUP1_{271-410}$ analyzed by SDS–PAGE and Coomassie; SEC performed on Superdex 200 10/300 GL. (**H**) Flotation assay for AUP1 reconstitution in ER-like liposomes. TM_{Cue1}-$AUP1_{271-410}$ co-migrates with liposomes to top fractions of a 0-40% (w/v) Nycodenz gradient; gradient fractions analyzed by SDS-PAGE and stain-free scanning. (**I**-**K**) Autoubiquitination of the E3 ligases RNF145 (I), RNF139 (J), and MARCHF6 (K) in the presence of indicated E2s and AUP1 (TM_{Cue1}-$AUP1_{271-410}$). Proteins were co-reconstituted in ER-like liposomes (E3/L = 1:8000, TM_{Cue1}-$AUP1_{271-410}$/L = 1:8000, UBE2J2/L = 1:32,000 (I, J); MARCH6 /L = 1:8000, TM_{Cue1}-$AUP1_{271-410}$/L = 1:8000, UBE2J2/L = 1:8000 (K); indicated reactions contained 2 μM UBE2G2. (**L**) Ubiquitin linkage type analysis in reactions with UBE2G2, AUP1 and RNF145 using ubiquitin mutants. ^{DL800}RNF145-ALFA and TM_{Cue1}-$AUP1_{271-410}$ were co-reconstituted in ER-like liposomes (P/L = 1:8000 each). Reactions ± 2 μM UBE2G2 were analyzed after 1 h by reducing SDS PAGE and fluorescence scanning. (**M**) Sodium hydroxide (NaOH) treatment to remove oxyester-linked ubiquitin from RNF139 in ER-like liposomes (^{DL800}RNF139-ALFA/L = 1:32,000, UBE2J2/L = 1:32,000). Samples collected at indicated times reduced with DTT, treated with 100 mM NaOH as indicated, and analyzed by SDS PAGE and fluorescence scanning. Detailed liposome compositions are given in Table 6.

Extended Data Figure 7 – E3-dependent and E3-independent ubiquitination and E2/E3 discharge assays (related to Fig. 5)

(**A**) Comparison of E3-dependent and –independent non-cysteine ubiquitination of $UBE2J2_{DL680}$ reconstituted in liposomes with indicated SFA content, with or without RNF145

(P/L = 1:32,000), after 10 min (see Fig. 2A, 5A for data). (**B**) Auto-ubiquitination of RNF139-ALFA with UBE2J2 in co-reconstituted liposomes with varying SFA content (^{DL800}RNF139-ALFA/L = 1:32,000, UBE2J2/L = 1:32,000. (**C**) Quantification of ubiquitinated RNF139 from (B) (n=2). (**D**) Ubiquitination of UBE2J2 by MARCHF6 in liposomes with the indicated SFA content (MARCH6-TEV-SBP$_{DL800}$/L = 1:32,000, UBE2J2$_{DL680}$/L = 1:32,000). (**E**) Quantification of ubiquitinated UBE2J2$_{DL680}$ in (D). (**F**) Purified ubiquitin-loaded UBE2G2 analyzed by non-reducing or reducing SDS–PAGE (nR, R) and Coomassie staining. Size-exclusion chromatography (Superdex 75 Increase 10/300 GL) with elution peak indicated (bracket). (**G**) E3-mediated discharge of fluorescent ubiquitin from UBE2G2. The indicated E3 ligases were co-reconstituted with AUP1 in liposomes with the indicated SFA content (E3 ligase/L = 1:16,000, TM$_{Cue1}$-AUP1$_{271-410}$/L= 1:16,000). R = reduced. Detailed liposome compositions are given in Table 6.

Extended Data Figure 8 – Characterization of SQLE, UBE2J2–E3 interactions, and ubiquitination in reconstituted systems (related to Fig. 5).

(**A**) Purified SQLE analyzed by SDS-PAGE and Coomassie staining. Size-exclusion chromatography (Superdex 200 10/30 GL) shows SQLE elution peak (bracket). (**B**) Flotation assay assessing SQLE reconstitution in liposomes with indicated SFA content. SQLE migrates with liposomes to the top fractions of a 0–40% (w/v) Nycodenz gradient; gradient fractions analyzed by SDS–PAGE and fluorescence scanning. (**C**) Interaction analysis between UBE2J2 and E3 ligase RNF145, reconstituted in the same or separate membranes. ^{DL800}RNF145-ALFA and UBE2J2$_{DL680}$ were individually or co-reconstituted in liposomes (P/L = 1:4000, SFA as indicated), mixed, solubilized, and subjected to immunoprecipitation of RNF145-ALFA using anti-ALFA nanobody. Elution was performed with 2× LDS sample buffer at 50°C or by Ulp1* protease. Proteins were analyzed by SDS–PAGE and fluorescence scanning. Numbers below the gel show fraction of co-purified UBE2J2$_{DL680}$, normalized to input. (**D**) Analysis of UBE2J2–RNF145-ALFA interaction at higher protein concentrations, by co-reconstitution (P/L = 1:4000, SFA as indicated) and anti-ALFA nanobody immunoprecipitation. Elution by Ulp1* protease; analysis by SDS–PAGE and fluorescence scanning. Numbers below the gel show co-purified UBE2J2$_{DL680}$ normalized to RNF145-ALFA and UBE2J2$_{DL680}$ input. (**E**) Auto-ubiquitination of RNF145-ALFA with UBE2J2 in liposomes with indicated SFA content at higher P/L ratios (^{DL800}RNF145-ALFA/L = 1:8000, UBE2J2/L = 1:8000) (**F**) Quantification of reactions in (E) (n=3). (**G**) Quantification of SQLE ubiquitination by MARCHF6 and UBE2J2. ^{DL800}SQLE, UBE2J2, and MARCHF6 were co-reconstituted in PC/PE liposomes with indicated SFA content (P/L = 1:16,000 each). (**H**) Quantification of UBE2J2$_{DL680}$ ubiquitin loading in the presence of MARCHF6. MARCHF6

co-reconstituted with $UBE2J2_{DL680}$ in liposomes with 10% SFA ($UBE2J2_{DL680}$/L = 1:32,000; MARCHF6/L as indicated). Detailed liposome compositions are given in Table 6.

Extended Data Figure 9 – Cholesterol-dependent regulation of RNF145 and related ubiquitination activity (related to Fig. 6)

(**A**) Steady state levels of RNF145 in HeLa cells under different sterol conditions. After 48 hours of growth under normal (5% FBS) or sterol deplete conditions (5% LPDS), 38 μM cholesterol complexed with β-methyl-cyclodextrin was supplemented in the medium for the indicated amounts of time. Whole cell lysates were analyzed by SDS PAGE and Western blotting. GAPDH served as a loading control. (**B**) Quantification of RNF145 levels from (A), normalized to GAPDH. (**C**) Auto-ubiquitination of ^{DL800}RNF145-ALFA with UBE2G2 in ER-like liposomes with or without 10 mol% cholesterol (^{DL800}RNF145-ALFA/L = 1:8000, TM_{Cue1}-$AUP1_{271-410}$/L = 1:8000). (**D**) Quantification of reactions in (C) (n=3). Statistical significance was assessed by Welch's two-sample t-test at each time point: *p = 0.0089, **p = 0.015, ***p = 0.110, ****p = 0.037. (**E**) Effect of cholesterol on RNF145-mediated discharge of fluorescent ubiquitin from UBE2G2. RNF145 was co-reconstituted with AUP1 in ER-like liposomes with or without 10 mol% cholesterol (^{DL800}RNF145-ALFA /L = 1:16,000, TM_{Cue1}-$AUP1_{271-410}$/L = 1:16,000). (**F**) Ubiquitination of catalytically inactive DL800RNF145^CS-ALFA in the presence of active RNF145 in ER-like liposomes with or without 10 mol% cholesterol (^{DL800}RNF145^{CS}-ALFA/L = 1:8000, RNF145-ALFA/L = 1:8000, UBE2J2/L = 1:32,000, TM_{Cue1}-$AUP1_{271-410}$/L = 1:32,000). **(G**) Quantification of ^{DL800} RNF145^{CS}-ALFA ubiquitination in (F) (n=3). Statistical significance by Welch's two-sample t-test at each time point: *p = 0.0001, **p = 0.018, ***p = 0.029, ****p = 0.032. Detailed liposome compositions are given in Table 6.

Extended Data Figure 10 – Comparison of sterol sensing domains (SSDs) among SCAP, HMGCR, RNF145, and RNF139 (related to Discussion).

(**A**) Structural alignment of the membrane domains of HMGCR (PDB: 8DJM) (Chen *et al.*, 2022) and SCAP (PDB: 7ETW) (Yan *et al*, 2021b). Both proteins display a kink in TM4 that forms a cleft capable of accommodating a sterol molecule (shown as sticks). (**B**) Alphafold2-predicted structures of the N-terminal domains of RNF145 (residues 1–307) and RNF139 (residues 1–321) reveal high similarity to each other, but marked differences from the SSDs of SCAP and HMGCR (Jumper *et al.*, 2021).

Figure 1

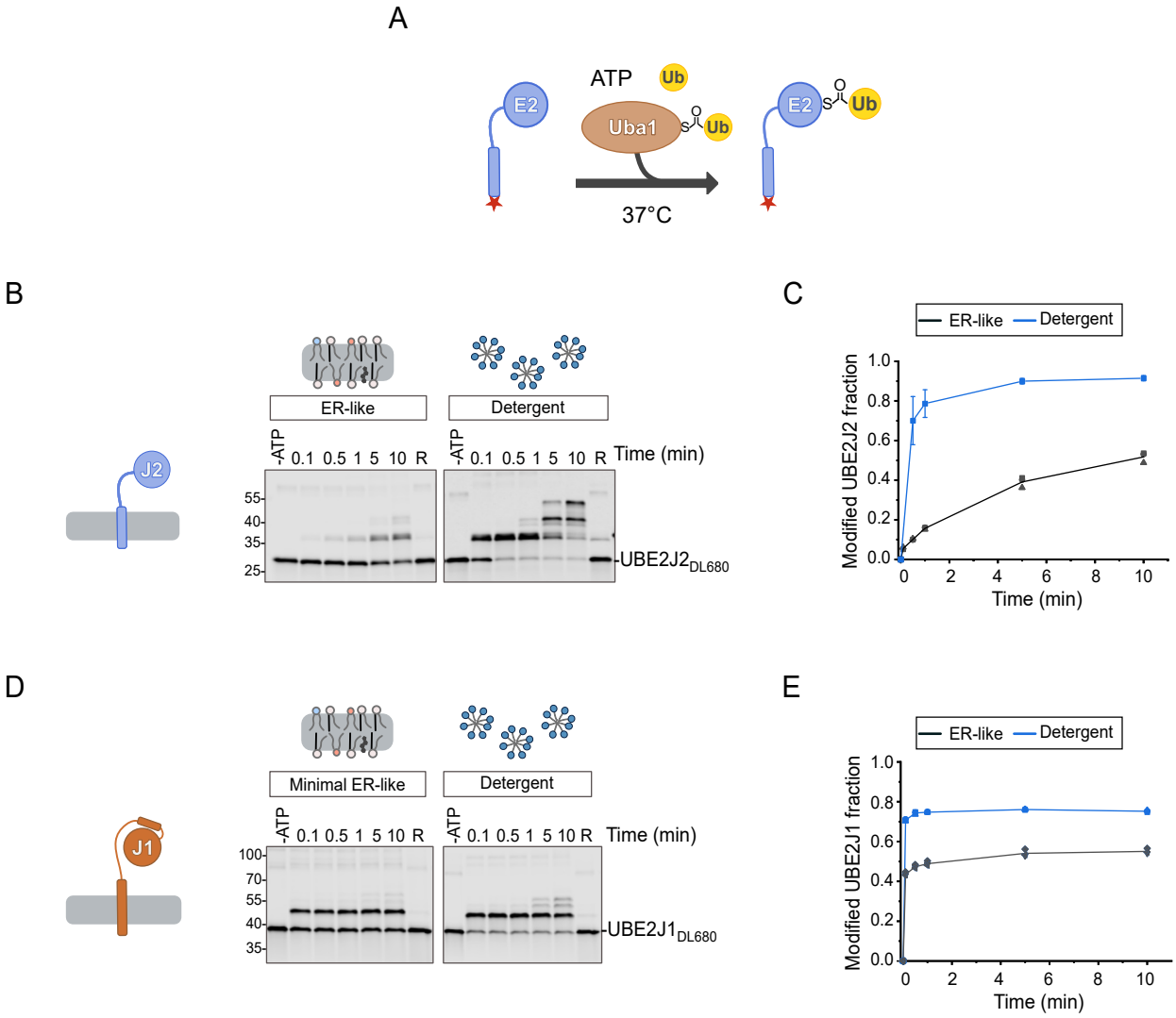
A
ATP
Ub
E2
Uba1
Ub
37°C
E2
Ub
B
ER-like
Detergent
-ATP
0.1 0.5 1 5 10 R
-ATP
0.1 0.5 1 5 10 R
Time (min)
J2
55
40
35
25
UBE2J2DL680
C
ER-like
Detergent
Modified UBE2J2 fraction
1.0
0.8
0.6
0.4
0.2
0.0
0 2 4 6 8 10
Time (min)
D
Minimal ER-like
Detergent
-ATP
0.1 0.5 1 5 10 R
-ATP
0.1 0.5 1 5 10 R
Time (min)
J1
100
70
55
40
35
UBE2J1DL680
E
ER-like
Detergent
Modified UBE2J1 fraction
1.0
0.8
0.6
0.4
0.2
0.0
0 2 4 6 8 10
Time (min)

Figure 2

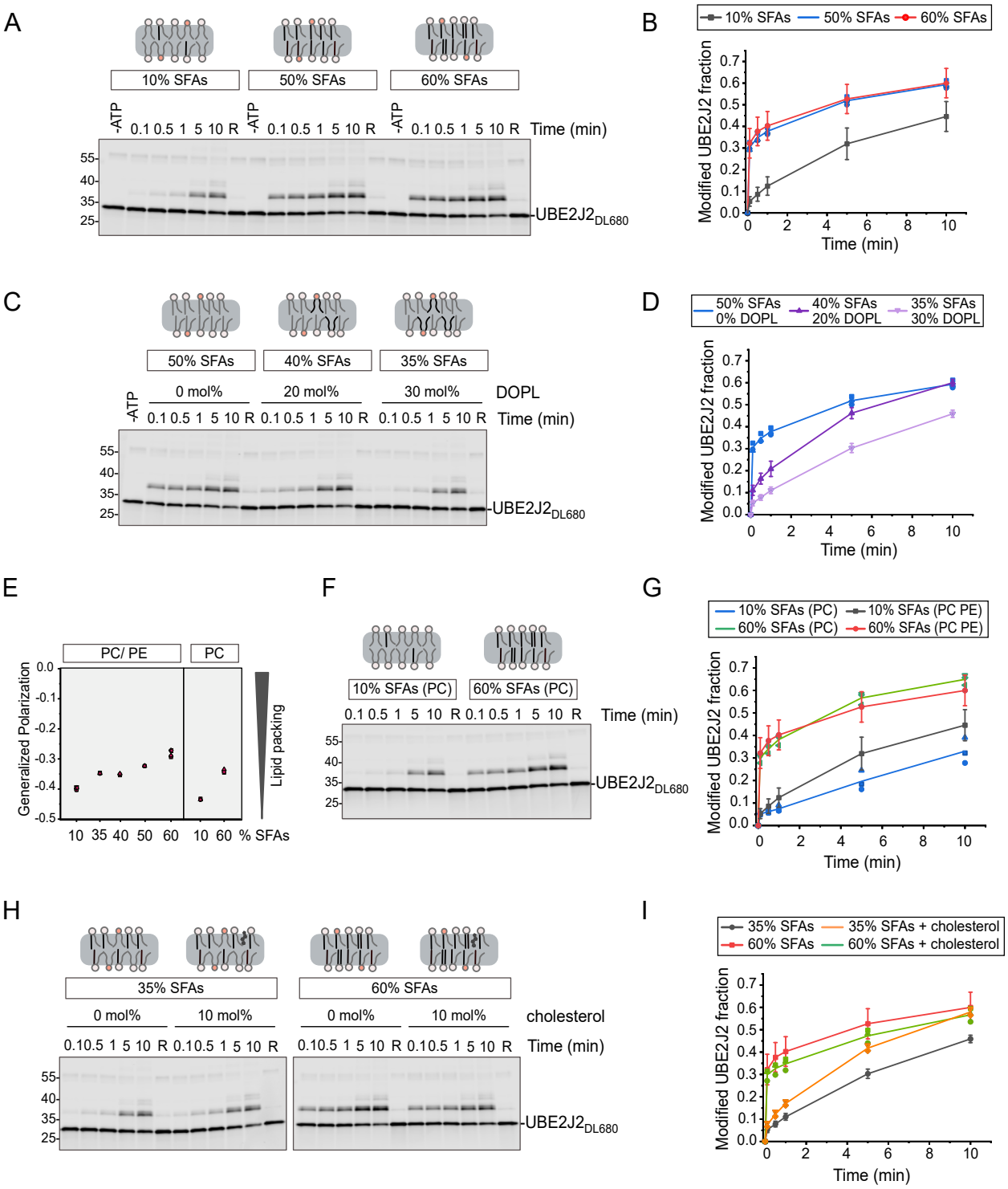
A
10% SFAs
50% SFAs
60% SFAs
-ATP
0.1 0.5 1 5 10 R
Time (min)
55-
40-
35-
25-
UBE2J2DL680
B
10% SFAs
50% SFAs
60% SFAs
Modified UBE2J2 fraction
Time (min)
C
50% SFAs
40% SFAs
35% SFAs
0 mol%
20 mol%
30 mol%
DOPL
D
50% SFAs 0% DOPL
40% SFAs 20% DOPL
35% SFAs 30% DOPL
E
PC/ PE
PC
Generalized Polarization
Lipid packing
10 35 40 50 60 10 60 % SFAs
F
10% SFAs (PC)
60% SFAs (PC)
G
10% SFAs (PC)
10% SFAs (PC PE)
60% SFAs (PC)
60% SFAs (PC PE)
H
35% SFAs
60% SFAs
0 mol%
10 mol%
cholesterol
I
35% SFAs
35% SFAs + cholesterol
60% SFAs
60% SFAs + cholesterol

Figure 3

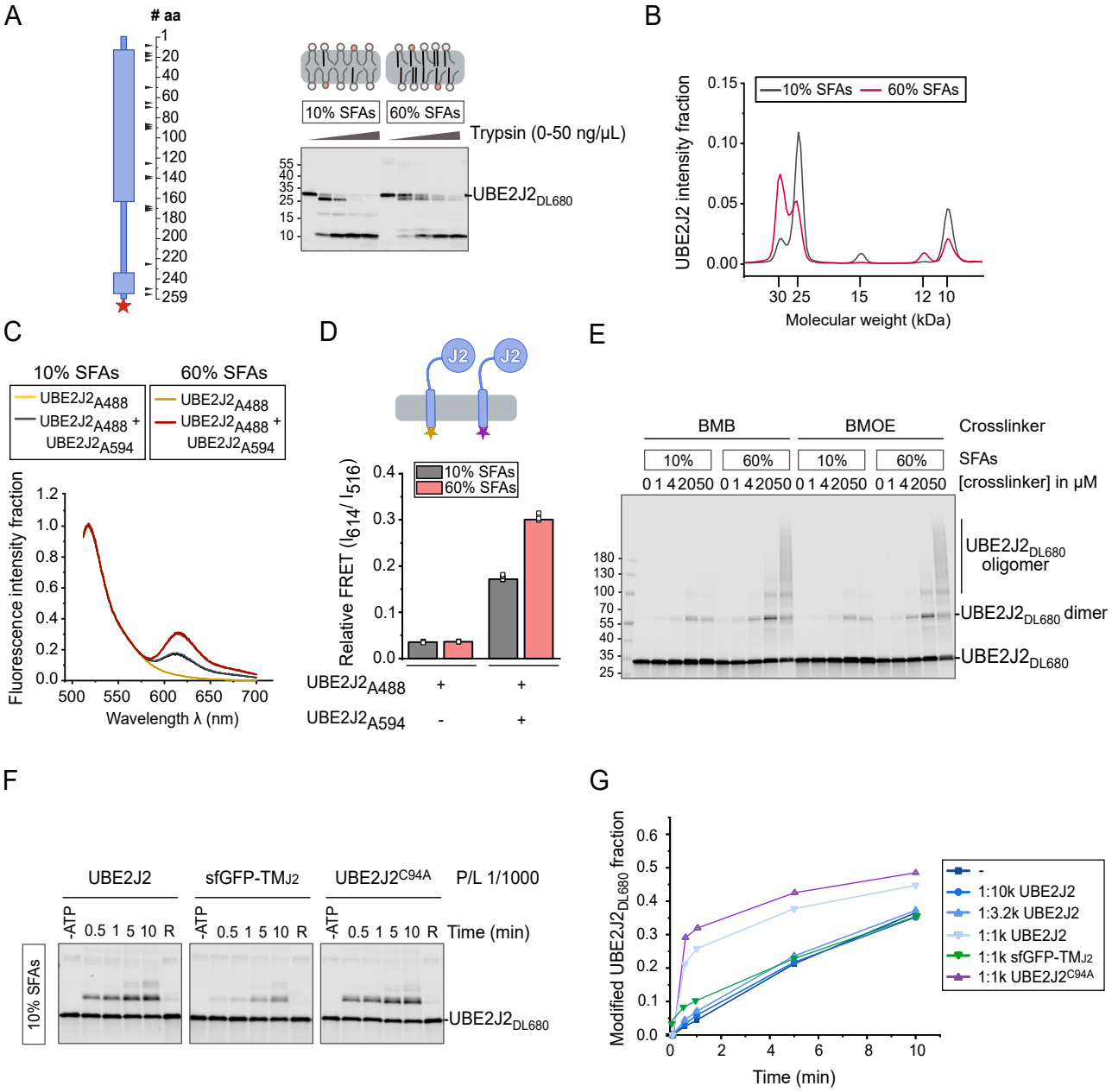
A
aa
1
20
40
60
80
100
120
140
160
180
200
220
240
259
10% SFAs
60% SFAs
Trypsin (0-50 ng/µL)
55
40
35
25
15
10
UBE2J2DL680
B
10% SFAs
60% SFAs
UBE2J2 intensity fraction
0.15
0.10
0.05
0.00
30 25
15
12 10
Molecular weight (kDa)
C
10% SFAs
60% SFAs
UBE2J2A488
UBE2J2A488 + UBE2J2A594
Fluorescence intensity fraction
1.2
1.0
0.8
0.6
0.4
0.2
0.0
500 550 600 650 700
Wavelength λ (nm)
D
J2
J2
Relative FRET (I614/ I516)
0.4
0.3
0.2
0.1
0.0
10% SFAs
60% SFAs
UBE2J2A488 + +
UBE2J2A594 - +
E
BMB
BMOE
Crosslinker
10%
60%
10%
60%
SFAs
0 1 4 20 50 0 1 4 20 50 0 1 4 20 50 0 1 4 20 50
[crosslinker] in µM
180
130
100
70
55
40
35
25
UBE2J2DL680 oligomer
UBE2J2DL680 dimer
UBE2J2DL680
F
UBE2J2
sfGFP-TMJ2
UBE2J2C94A
P/L 1/1000
-ATP 0.5 1 5 10 R
-ATP 0.5 1 5 10 R
-ATP 0.5 1 5 10 R
Time (min)
10% SFAs
UBE2J2DL680
G
Modified UBE2J2DL680 fraction
0.6
0.5
0.4
0.3
0.2
0.1
0.0
0 2 4 6 8 10
Time (min)
-
1:10k UBE2J2
1:3.2k UBE2J2
1:1k UBE2J2
1:1k sfGFP-TMJ2
1:1k UBE2J2C94A

Figure 4

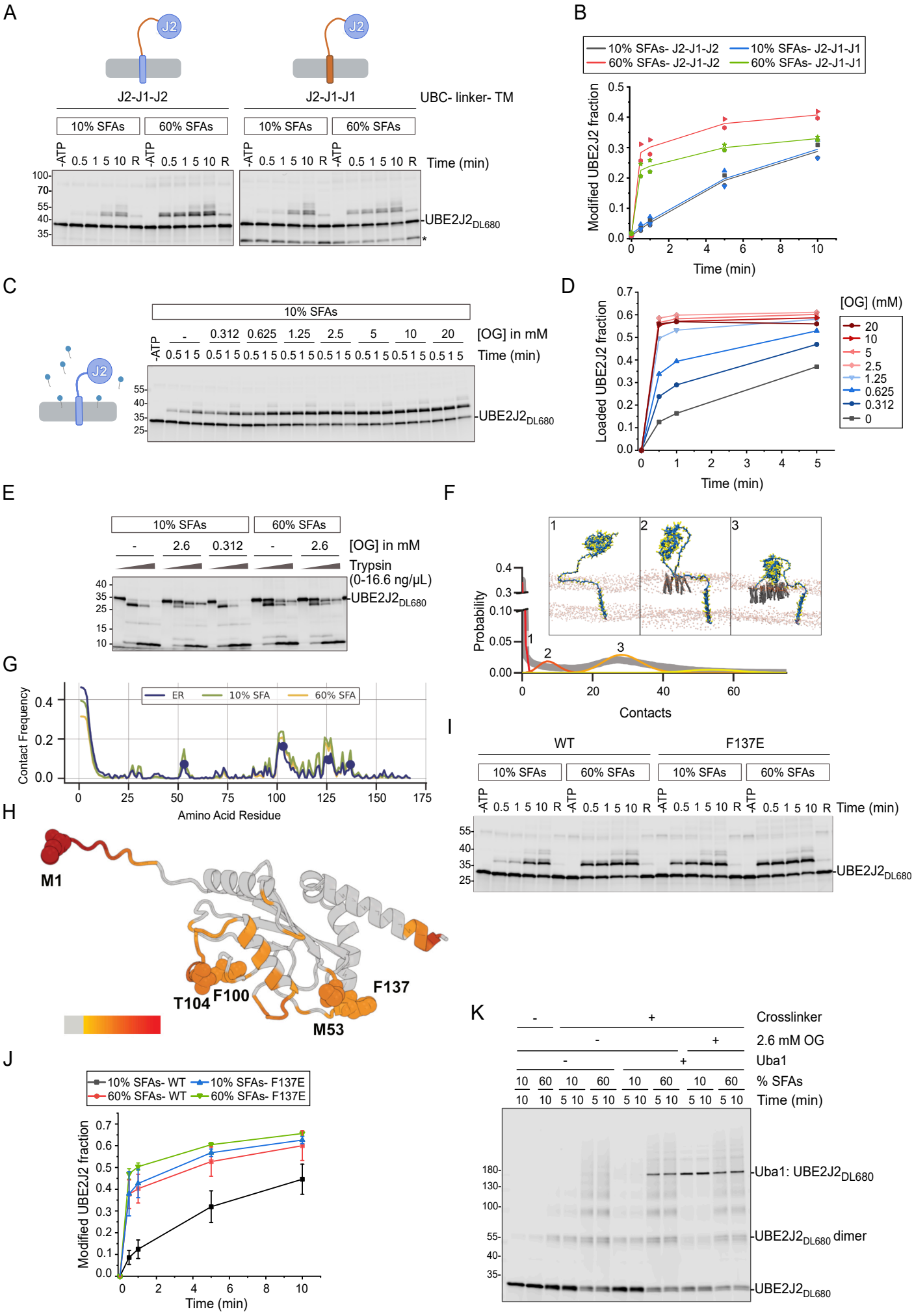
A
J2
J2-J1-J2
J2-J1-J1
UBC- linker- TM
10% SFAs
60% SFAs
-ATP 0.5 1 5 10 R
Time (min)
UBE2J2DL680
B
10% SFAs- J2-J1-J2
60% SFAs- J2-J1-J2
10% SFAs- J2-J1-J1
60% SFAs- J2-J1-J1
Modified UBE2J2 fraction
Time (min)
C
10% SFAs
[OG] in mM
0.312 0.625 1.25 2.5 5 10 20
Time (min)
UBE2J2DL680
D
Loaded UBE2J2 fraction
Time (min)
[OG] (mM)
20
10
5
2.5
1.25
0.625
0.312
0
E
10% SFAs
60% SFAs
[OG] in mM
Trypsin (0-16.6 ng/µL)
UBE2J2DL680
F
Probability
Contacts
G
Contact Frequency
ER
10% SFA
60% SFA
Amino Acid Residue
H
M1
T104
F100
M53
F137
I
WT
F137E
10% SFAs
60% SFAs
-ATP 0.5 1 5 10 R
Time (min)
UBE2J2DL680
J
10% SFAs- WT
10% SFAs- F137E
60% SFAs- WT
60% SFAs- F137E
Modified UBE2J2 fraction
Time (min)
K
Crosslinker
2.6 mM OG
Uba1
% SFAs
Time (min)
Uba1: UBE2J2DL680
UBE2J2DL680 dimer
UBE2J2DL680

Figure 5

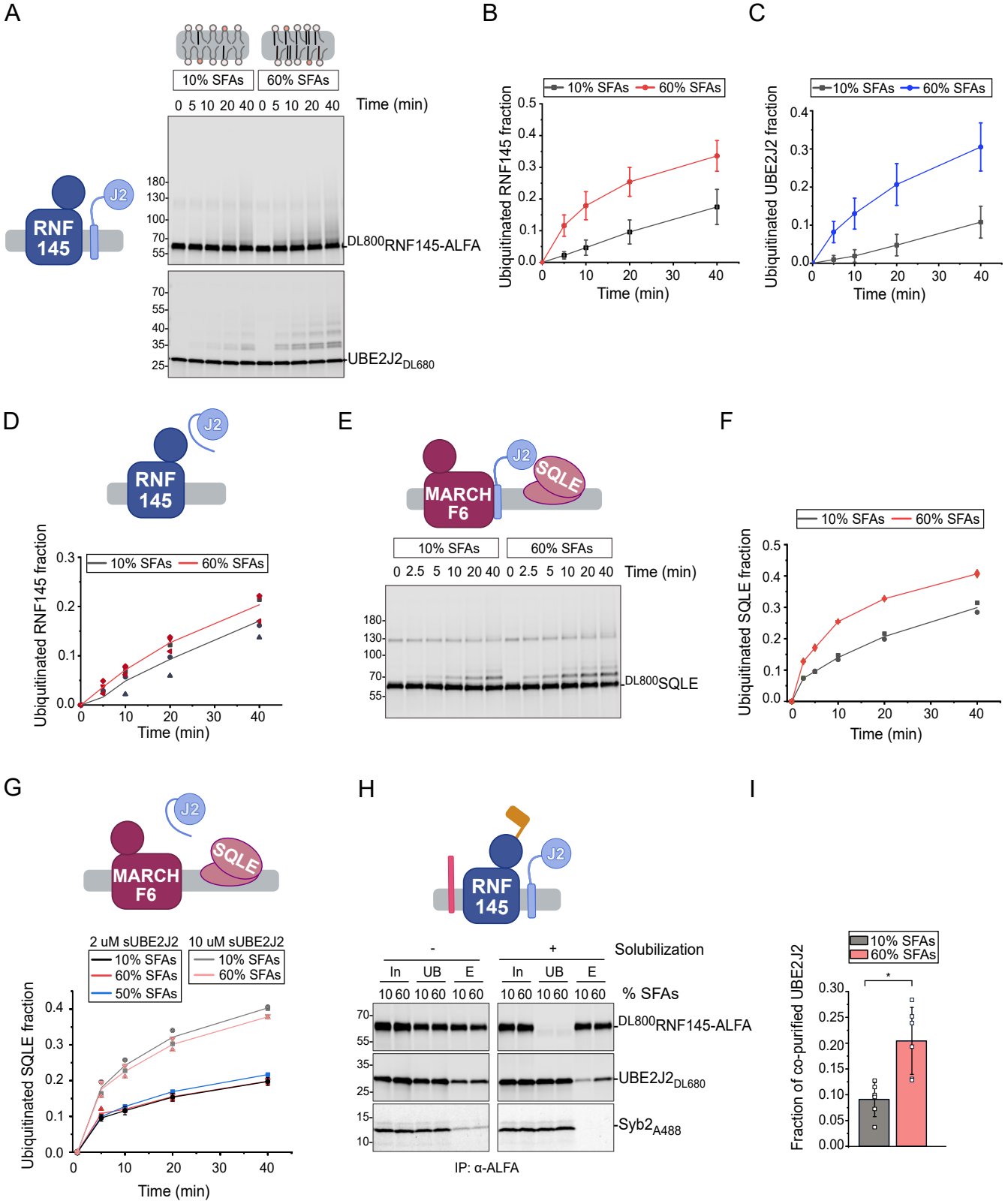
A
10% SFAs
60% SFAs
0 5 10 20 40 0 5 10 20 40
Time (min)
RNF 145
J2
DL800RNF145-ALFA
UBE2J2DL680
B
10% SFAs
60% SFAs
Ubiquitinated RNF145 fraction
Time (min)
C
Ubiquitinated UBE2J2 fraction
D
Ubiquitinated RNF145 fraction
E
MARCH F6
SQLE
0 2.5 5 10 20 40 0 2.5 5 10 20 40
DL800SQLE
F
Ubiquitinated SQLE fraction
G
2 uM sUBE2J2
10 uM sUBE2J2
50% SFAs
H
Solubilization
In UB E In UB E
% SFAs
Syb2A488
IP: α-ALFA
I
Fraction of co-purified UBE2J2

Figure 6

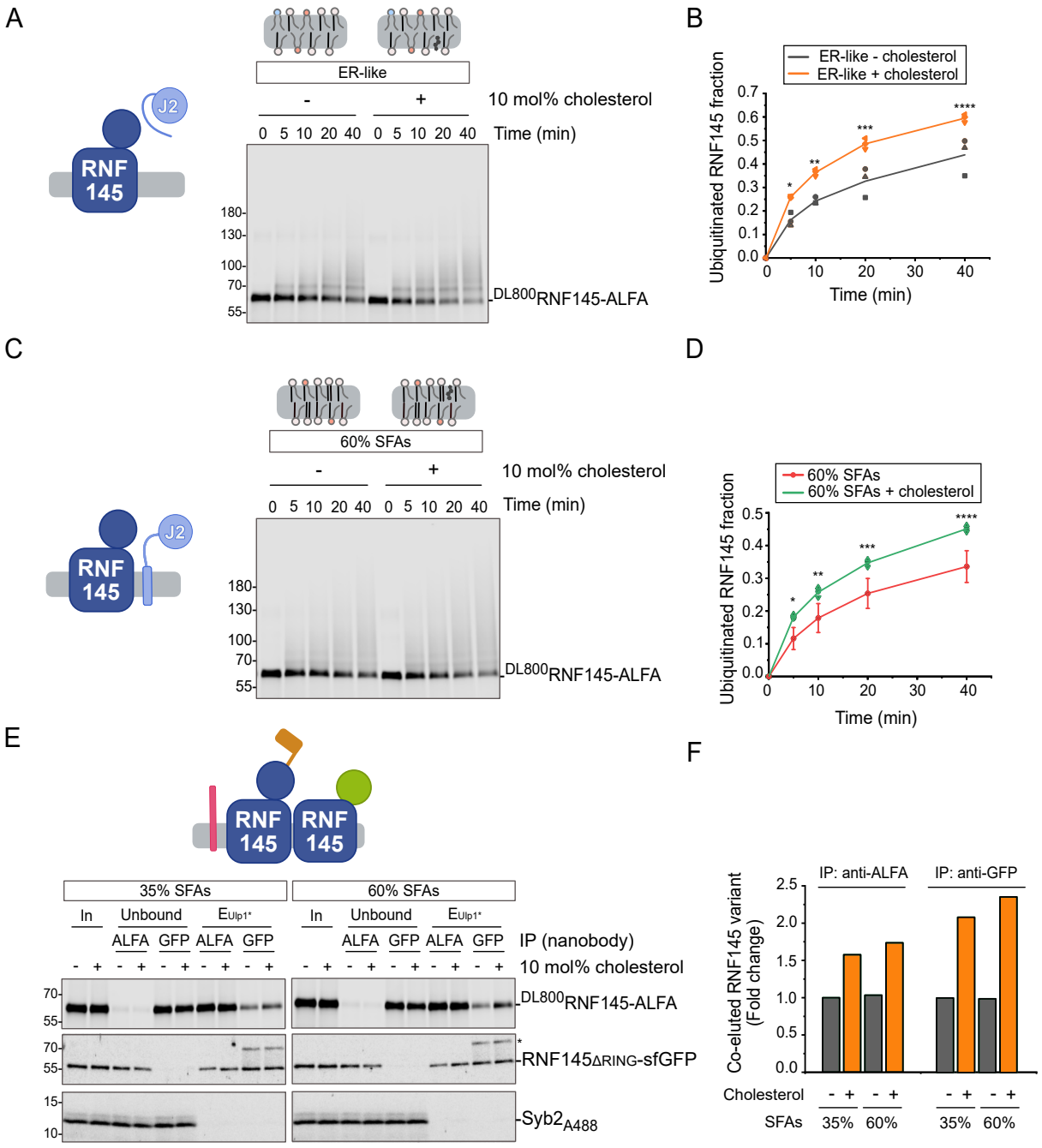
A
ER-like
-
+
10 mol% cholesterol
0 5 10 20 40 0 5 10 20 40
Time (min)
J2
RNF 145
180-
130-
100-
70-
55-
DL800RNF145-ALFA
B
ER-like - cholesterol
ER-like + cholesterol
Ubiquitinated RNF145 fraction
Time (min)
C
60% SFAs
-
+
10 mol% cholesterol
0 5 10 20 40 0 5 10 20 40
Time (min)
J2
RNF 145
180-
130-
100-
70-
55-
DL800RNF145-ALFA
D
60% SFAs
60% SFAs + cholesterol
Ubiquitinated RNF145 fraction
Time (min)
E
RNF 145
RNF 145
35% SFAs
60% SFAs
In
Unbound
Eulp1*
ALFA
GFP
IP (nanobody)
10 mol% cholesterol
DL800RNF145-ALFA
RNF145ΔRING-sfGFP
Syb2A488
F
IP: anti-ALFA
IP: anti-GFP
Co-eluted RNF145 variant (Fold change)
Cholesterol
SFAs
35%
60%

Figure 7

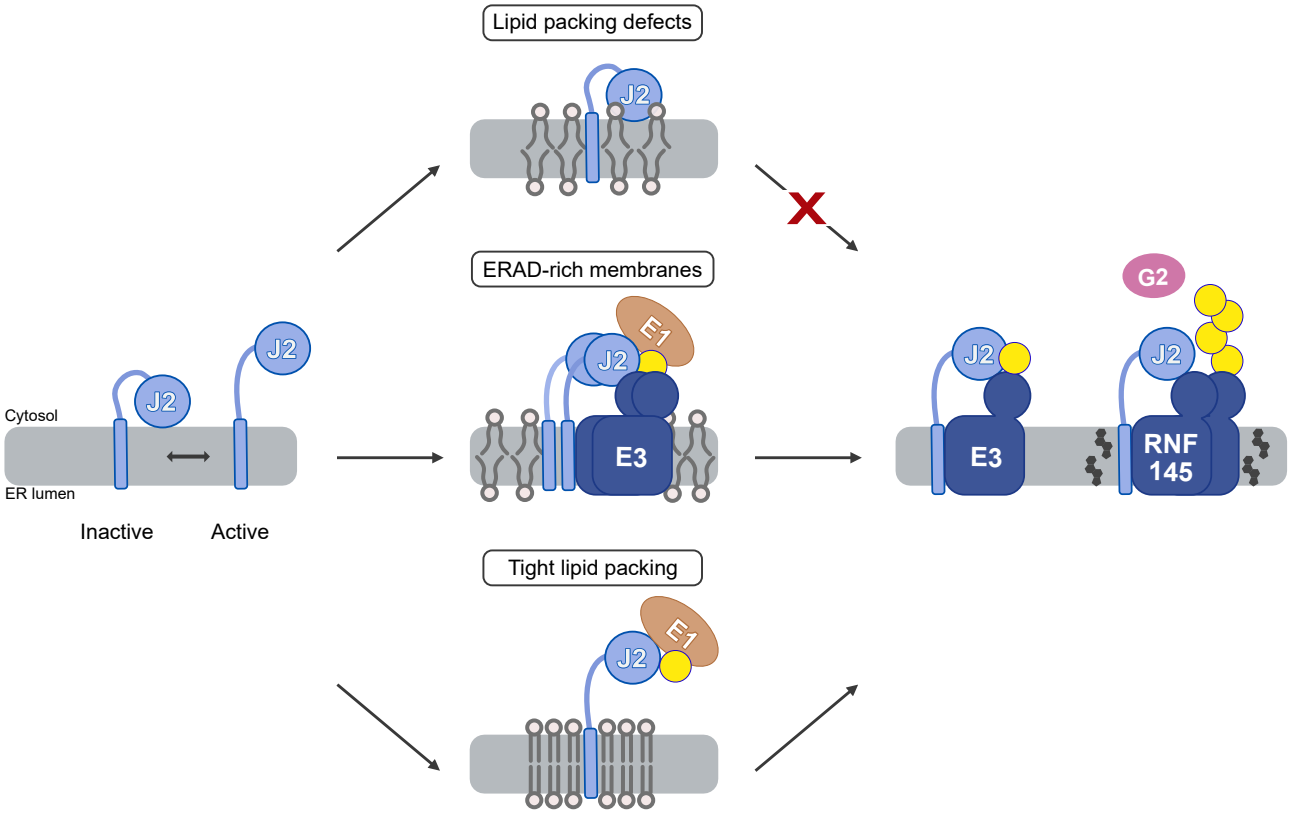
Lipid packing defects
J2
ERAD-rich membranes
E1
J2
E3
G2
J2
J2
E3
RNF
145
Cytosol
ER lumen
J2
J2
Inactive
Active
Tight lipid packing
E1
J2

Extended Data Figure 1 - related to Figure 1

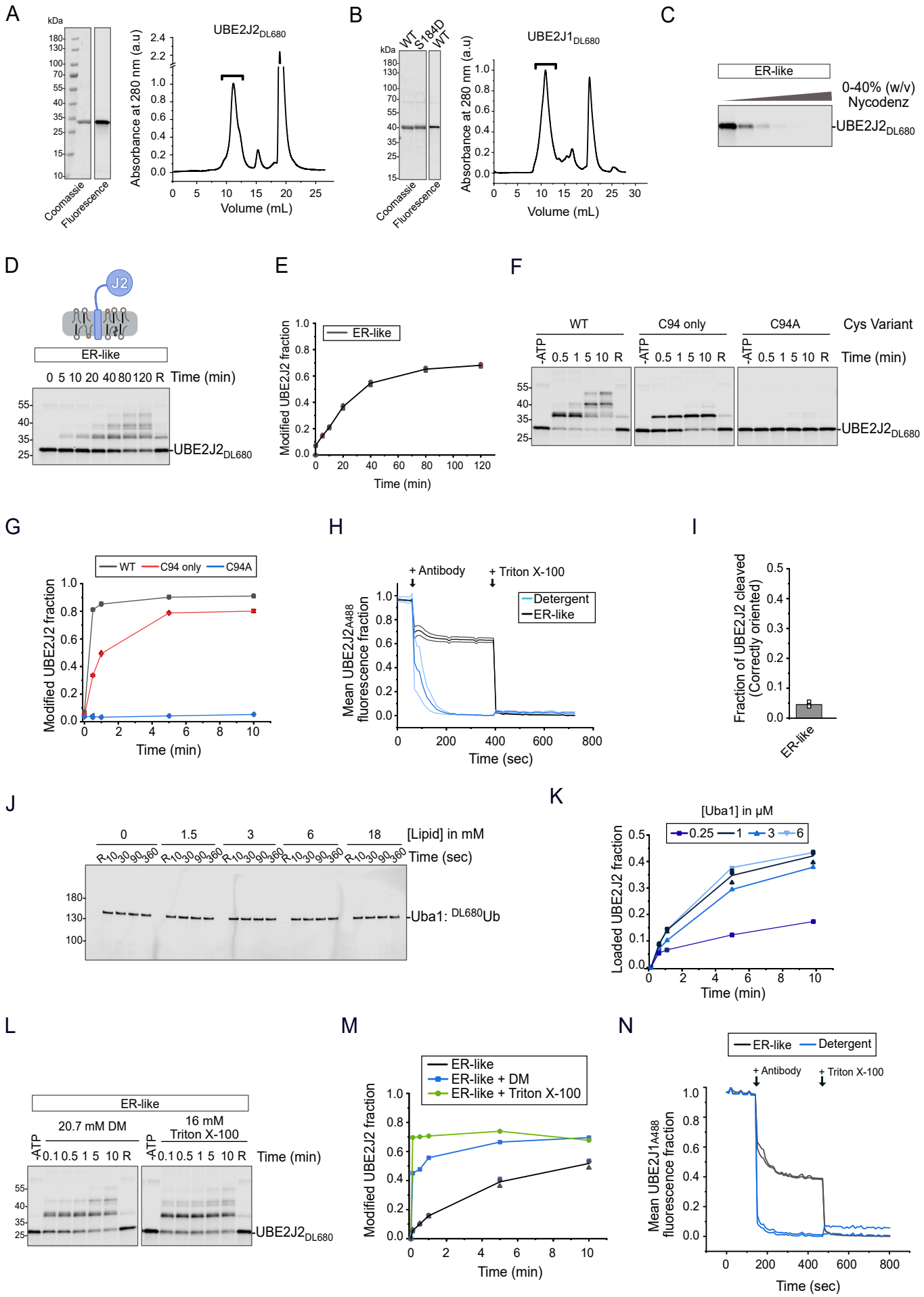

Extended Data Figure 2 - related to Figure 2

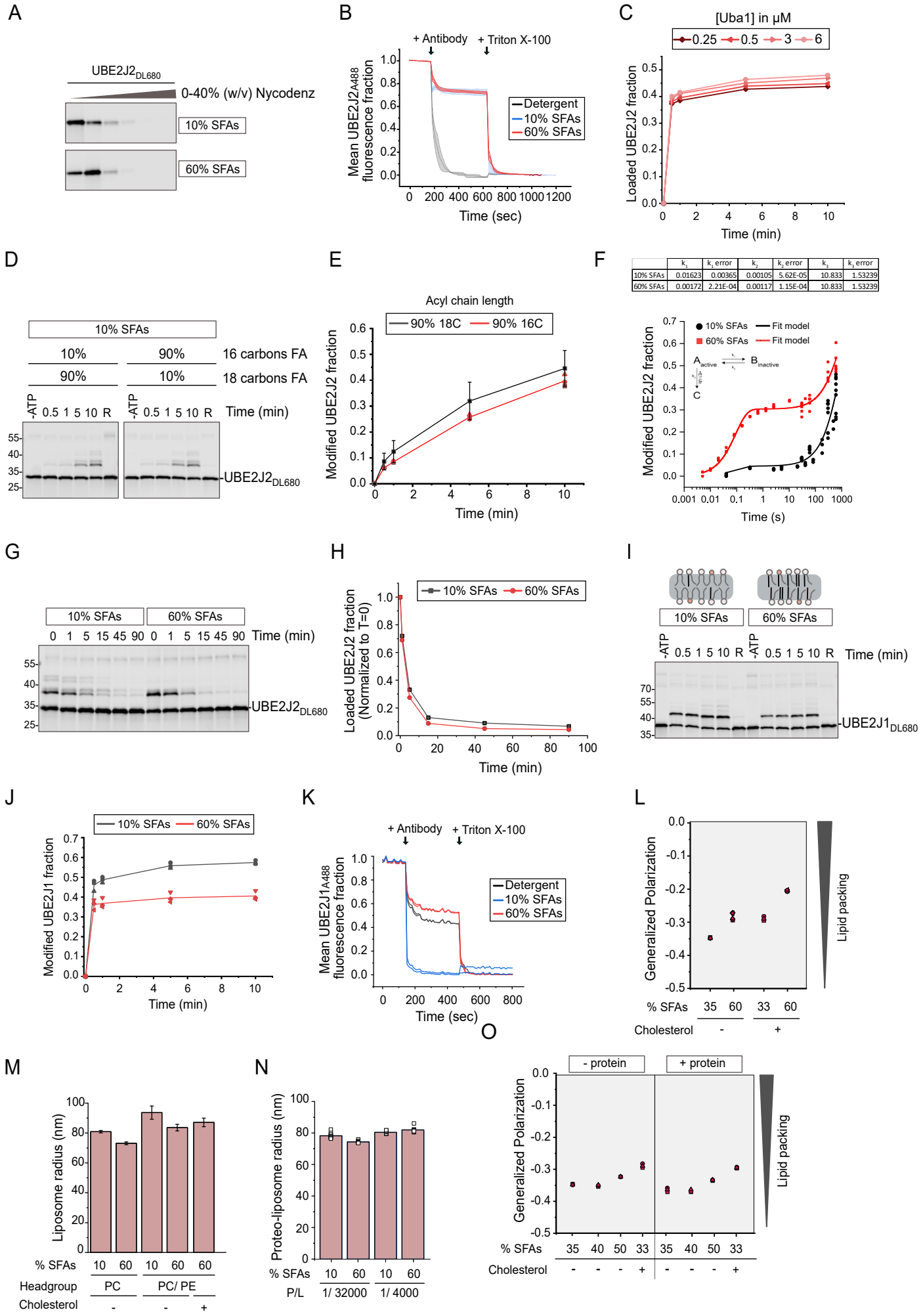

	k_1	k_1 error	k_2	k_2 error	k_3	k_3 error
10% SFAs	0.01623	0.00365	0.00105	5.62E-05	10.833	1.53239
60% SFAs	0.00172	2.21E-04	0.00117	1.15E-04	10.833	1.53239

Extended Data Figure 3 - related to Figure 3

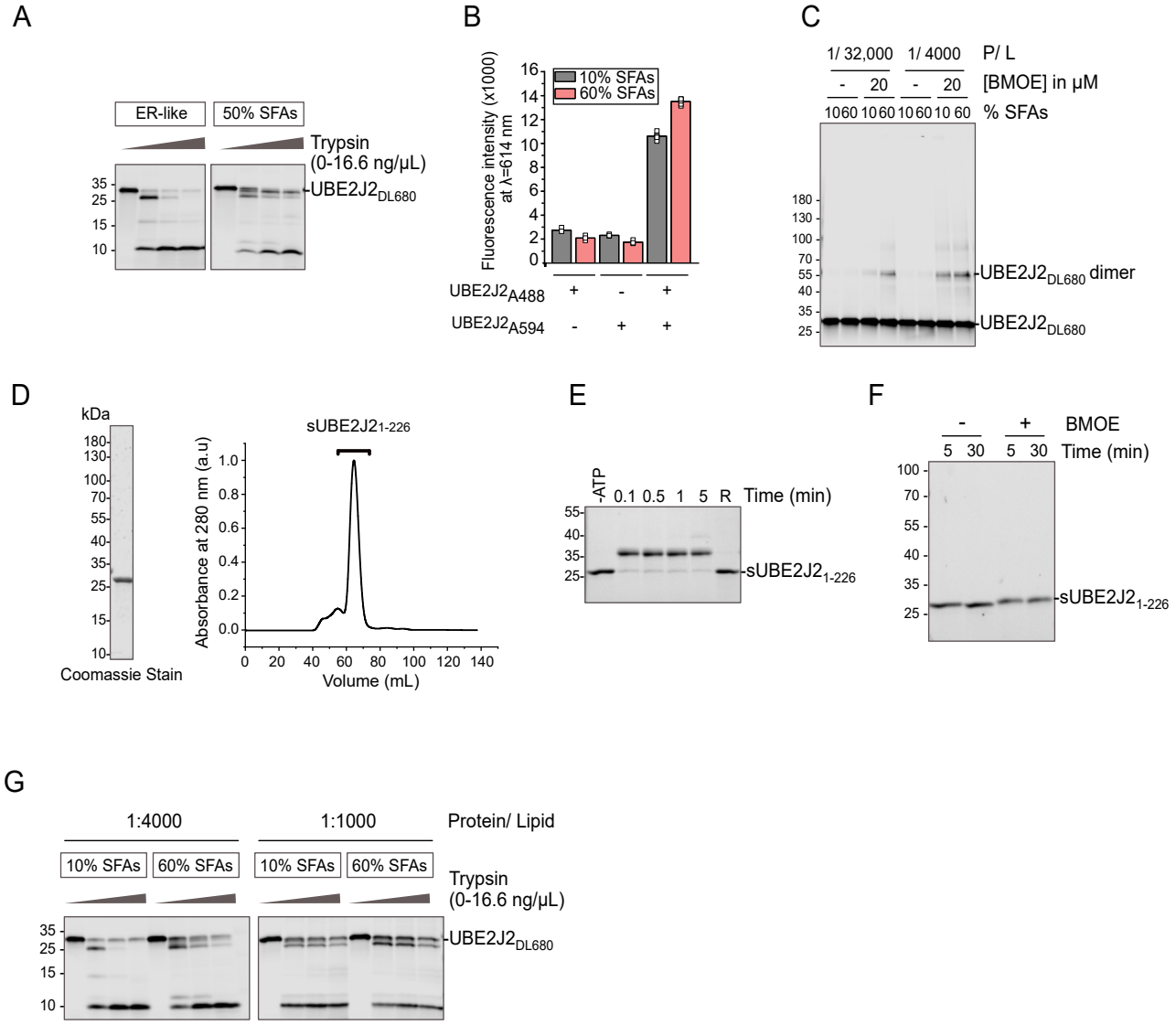

Extended Data Figure 4 - related to Figure 4

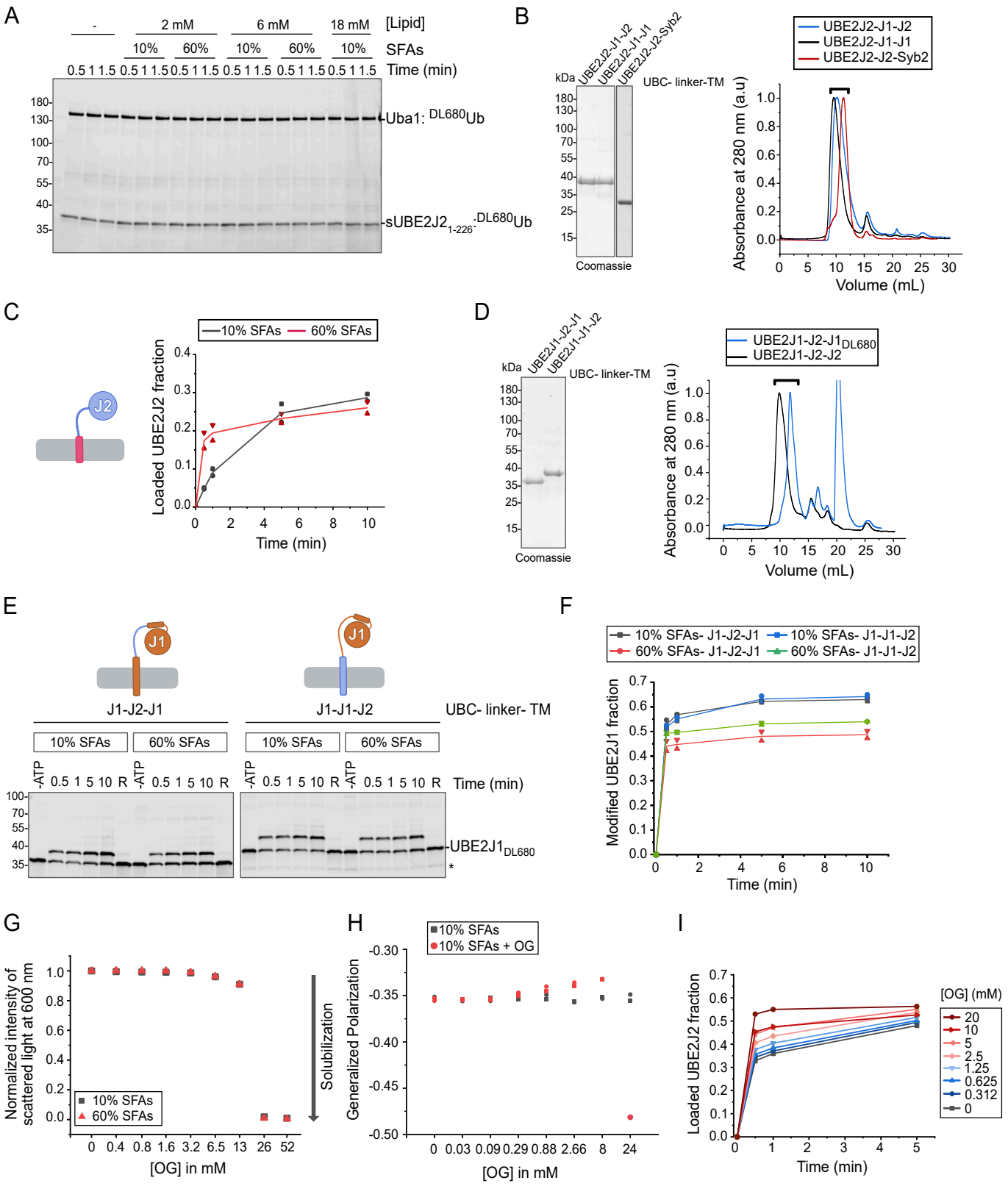

Extended Data Figure 5 - related to Figure 4

A

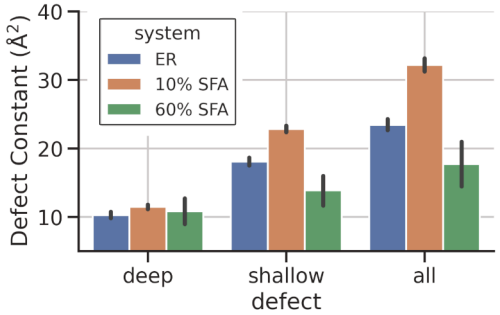

B

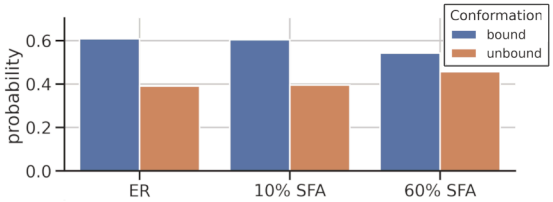

C

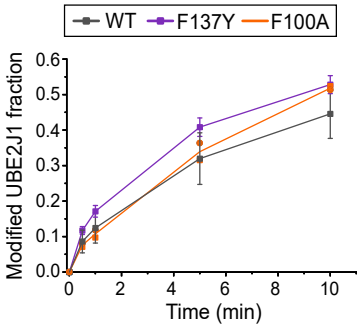

D

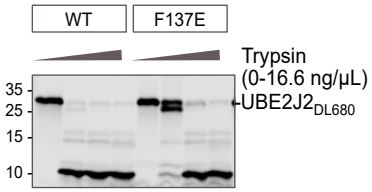

E

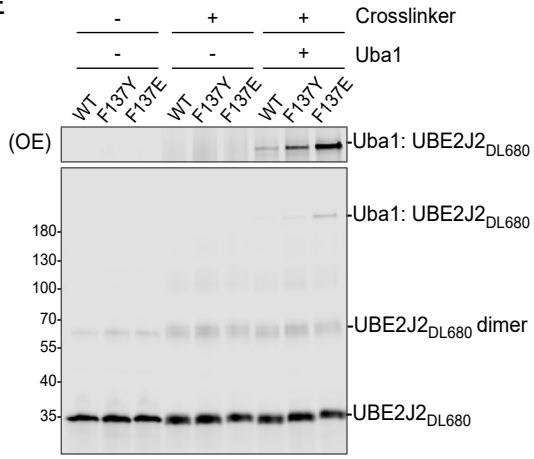

Extended Data Figure 6 - related to Figure 5

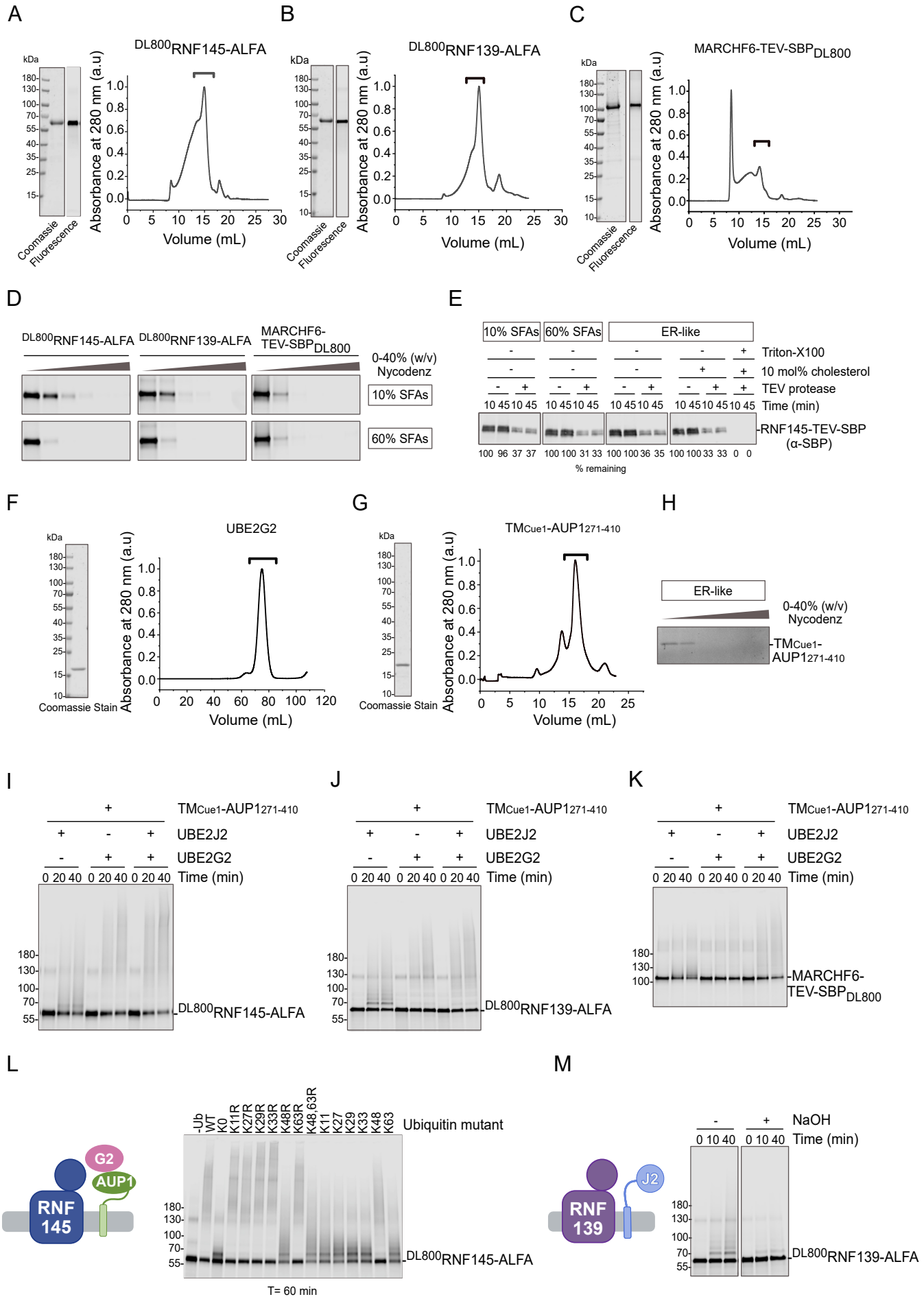

Extended Data Figure 7 - related to Figure 5

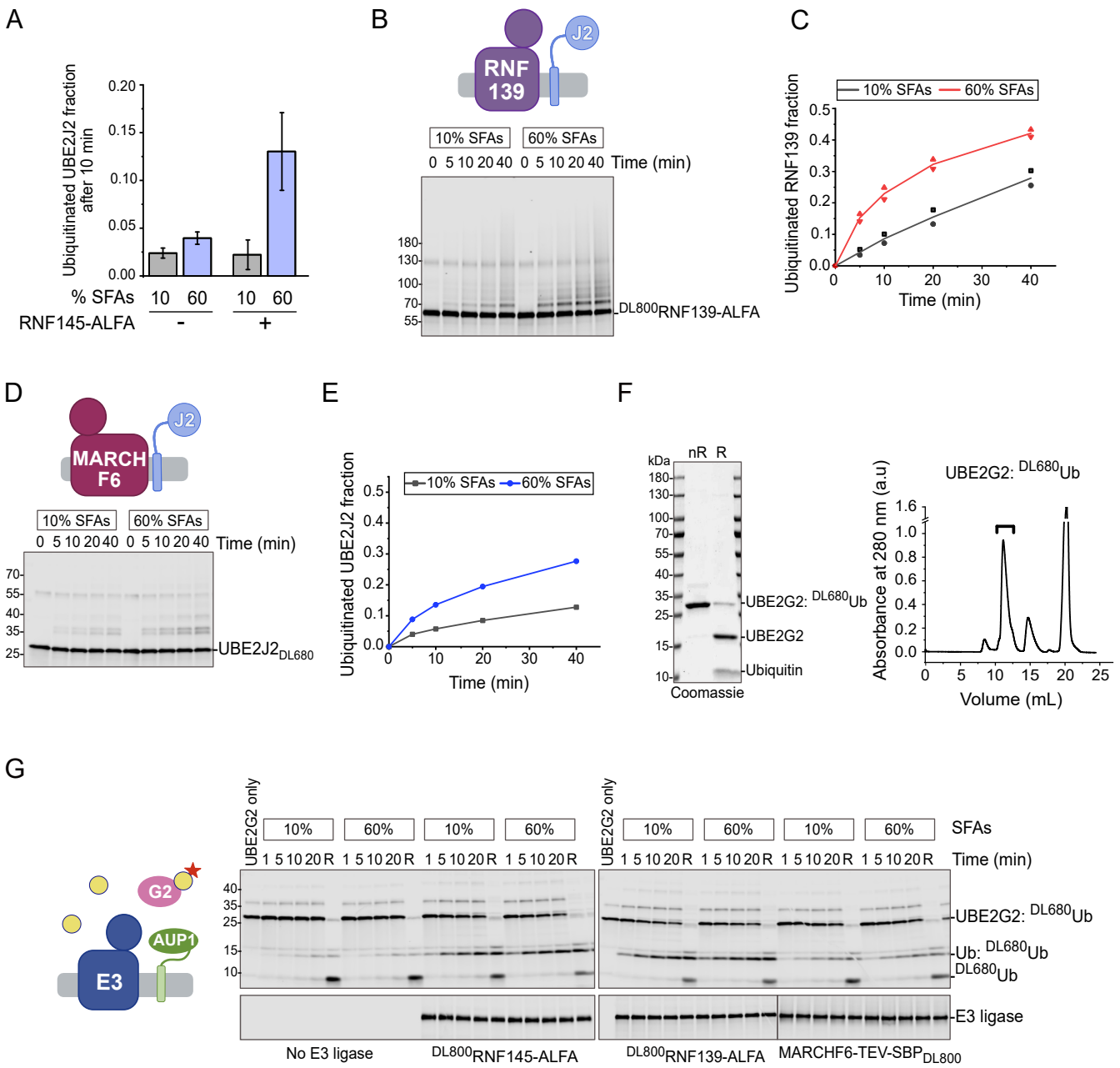

Extended Data Figure 8 - related to Figure 5

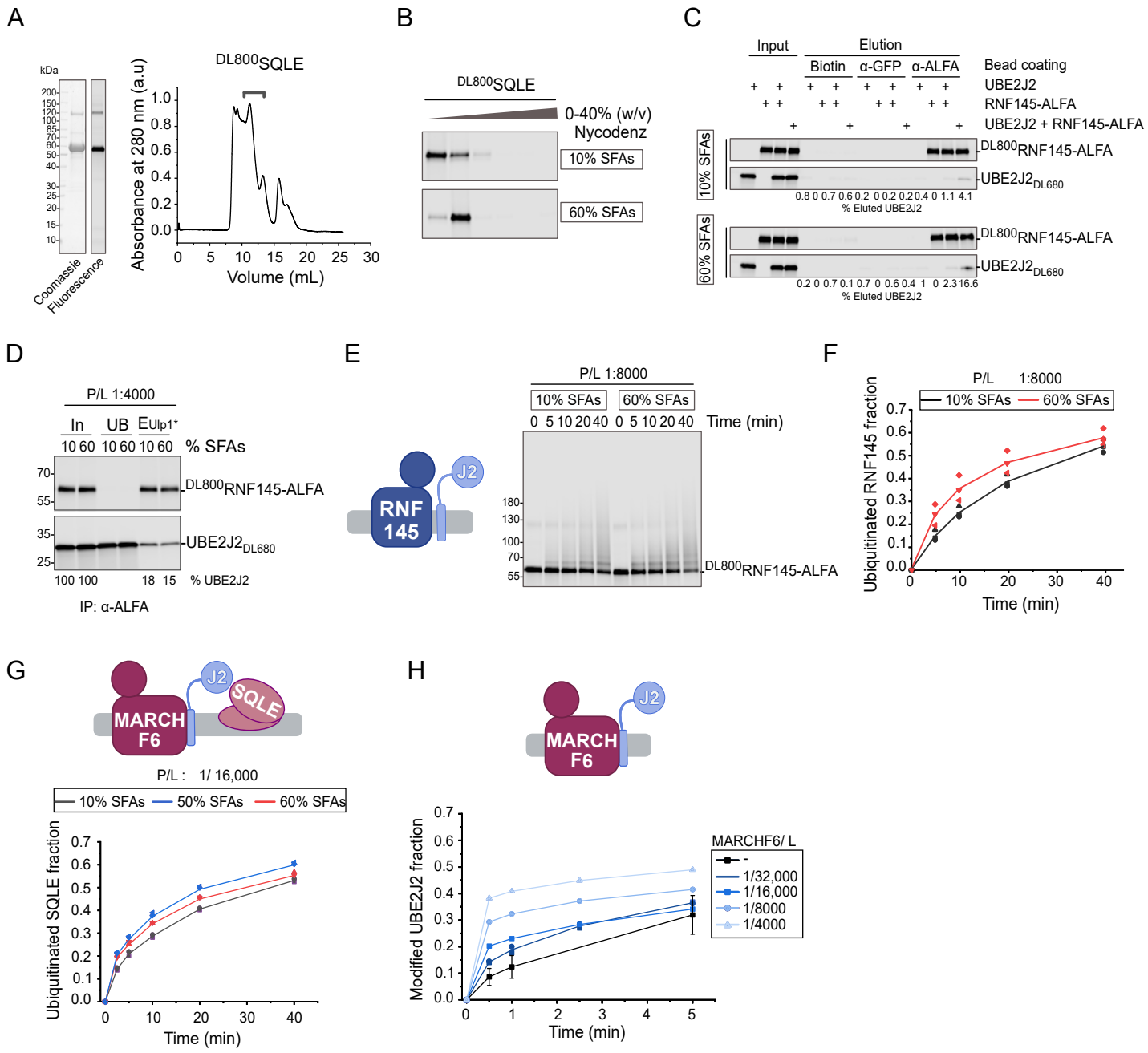

Extended Data Figure 9 - related to Figure 6

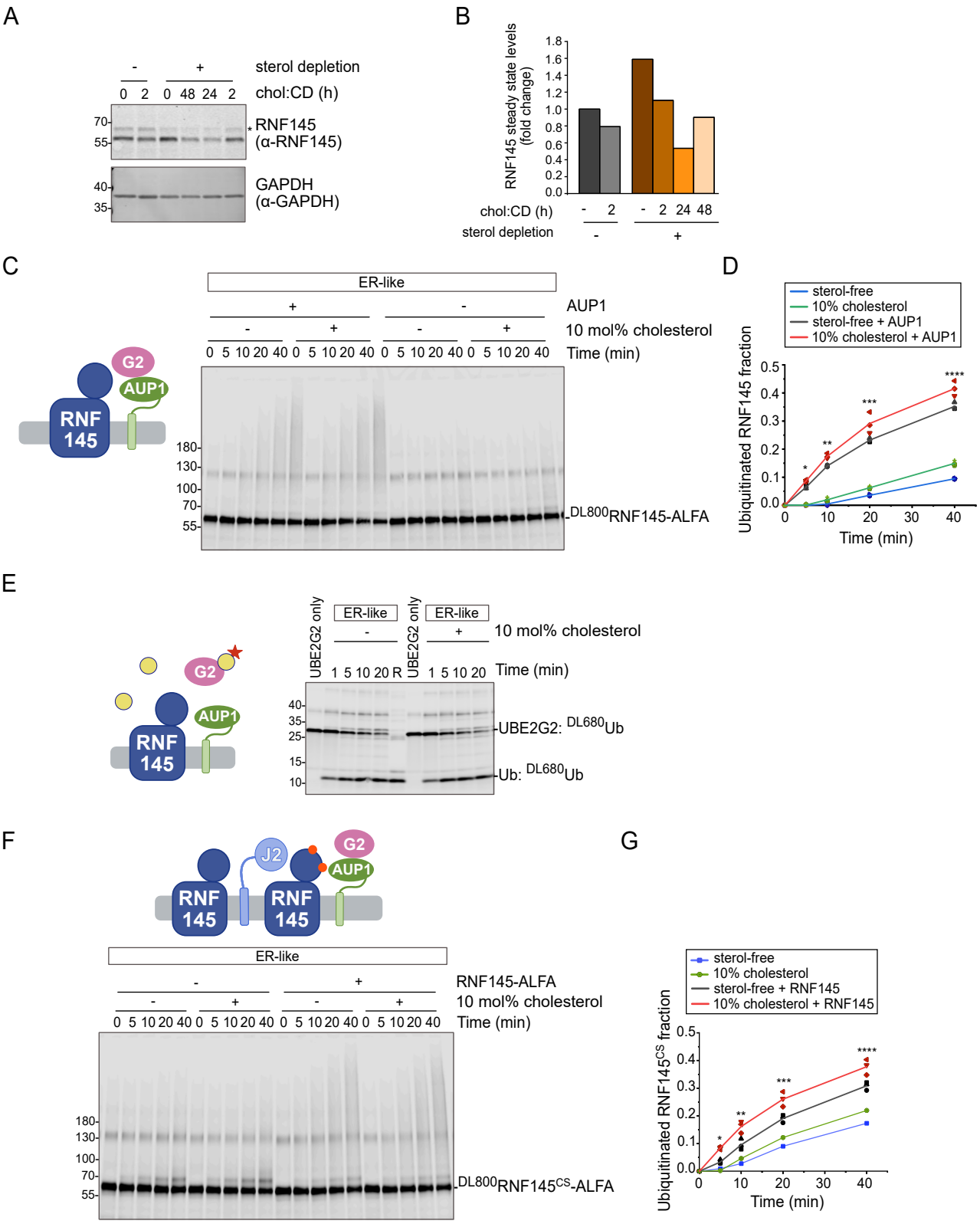
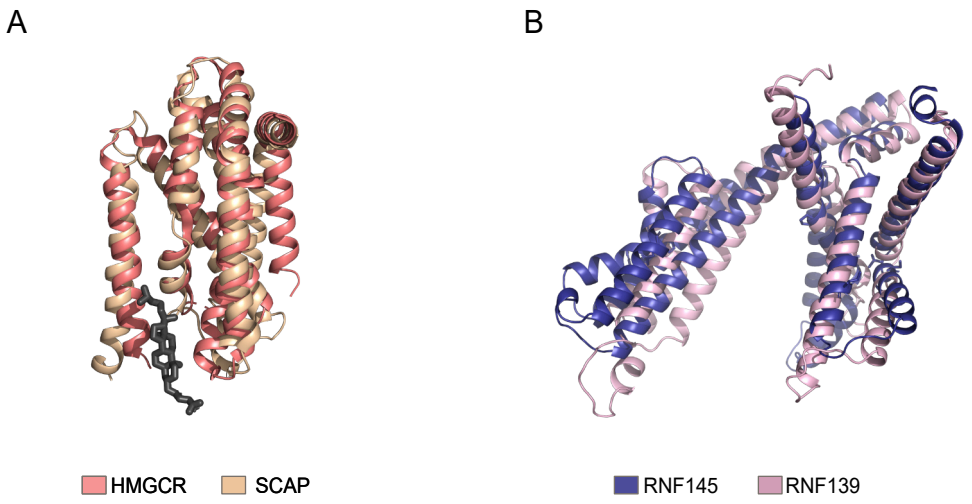
Extended Data Figure 10 - related to Discussion